AFCRL-69-0089

LUNAR SURFACE STUDIES

David G. Murcray

Department of Physics

University of Denver

Denver, Colorado 80210

Contract No. AF 19(628)-4797

Project No. 8602

Task No. 860202

Work Unit No. 86020201

FINAL REPORT

17 May 1965 through 16 January 1969

January 1969

Contract Monitor: Joel E. M. Adler

Space Physics Laboratory

Prepared for

AIR FORCE CAMBRIDGE RESEARCH LABORATORIES

OFFICE OF AEROSPACE RESEARCH

UNITED STATES AIR FORCE

BEDFORD, MASSACHUSETTS 01730

AFCRL-69-0089

LUNAR SURFACE STUDIES

David G. Murcray

Department of Physics

University of Denver

Denver, Colorado 80210

Contract No. AF 19(628)-4797

Project No. 8602

Task No. 860202

Work Unit No. 86020201

FINAL REPORT

17 May 1965 through 16 January 1969

January 1969

Contract Monitor: Joel E. M. Adler

Space Physics Laboratory

Prepared for

AIR FORCE CAMBRIDGE RESEARCH LABORATORIES

OFFICE OF AEROSPACE RESEARCH

UNITED STATES AIR FORCE

BEDFORD, MASSACHUSETTS 01730

ABSTRACT

This report presents the results of a number of investigations, the common goal of which was a better understanding of the lunar surface. These studies have included measuring the infrared emissivity of various areas of the lunar surface in the wavelength region from 7μ to 14μ with a balloon borne system and laboratory studies of the behavior of various materials under simulated lunar environment. The laboratory studies have included the role of sintering in the mechanical properties of lunar surface, techniques for measuring the adhesive properties of fresh surfaces in a high vacuum environment, development of proton beams which can give reasonable proton fluxes in a high vacuum environment for the study of the effect of protons on lunar surface materials and finally the possibility of using X-ray topography as a tool for studying proton damaged surfaces.

TABLE OF CONTENTS

TABLE OF CONTENTS
(Cont'd)

LIST OF FIGURES

1. INTRODUCTION

The lunar surface has been the subject of considerable research over the years and has received particular attention during the last decade. Most of these investigations have been made remotely either via ground based or satellite based instruments. These efforts have yielded considerable information concerning the lunar surface however in some cases the results have been unexpected and currently have not been properly explained.

The material of the lunar surface is subjected to extremes of environment quite different from that of a similar surface material on earth. In view of this it is quite possible that the surface may be modified by its environment and hence exhibit characteristics which are different from those exhibited by a similar material found on earth.

This contract had the rather broad objective of increasing our knowledge of the lunar surfa e. A number of investigations have been undertaken toward this end. These have included laboratory studies under a simulated lunar environment, a study of the infrared radiation emitted by selected features of the lunar surface and the proper preparation of samples for the laboratory studies. Some of the laboratory studies were discontinued either because they were not yielding meaningful results or else additional experimental data became available which eliminated the need for the particular study. The major studies undertaken during this program which have yielded information concerning the lunar surface or will aid in future investigations are summarized below. These investigations have been conducted by a number of separate groups at the University of Denver and the summaries have been written by different authors. These separate summaries have not been edited but are included as written by the principal investigator of the various studies. Thus there will be some overlap in the discussions and some nonuniformity of style of the various sections.

2. LUNAR INFRARED EMISSION STUDIES

This portion of the program involved investigation of problems related to rock and mineral identification by thermal emission spectral measurements. Major emphasis has been on obtaining emission spectra of selected areas of the lunar surface with sufficient accuracy to permit identification of lunar surface materials. Secondary efforts have been aimed at construction of instrumentation for laboratory measurements of silicate emission spectra for comparison with the lunar data and at measurements of terrestrial surface emissions from balloon altitude.

2.1 Terrestrial Emission Measurements

The identification of rocks and minerals on the earth's surface through emission spectra taken from satellites or airborne vehicles is likely to present a more difficult problem than similar studies on extraterrestrial bodies. The presence of an atmosphere comparatively rich in infrared active gases and the effects of weathering and vegetative growth all tend to limit the accuracy with which such measurements can be made. On the other hand the solid form of the materials on the earth as opposed to the evidently dust covered surface of the moon can reduce the accuracy required in the measurement.

As a test of the feasibility of this sort of measurement, both for the earth's surface and for other bodies surrounded by atmospheres, a balloon borne spectral radiometer which scanned the region from 8.5μ to 14μ was designed and constructed. The field of view of the radiometer was restricted by foreoptics to 2x5 millradians.

The equipment was flown on 5 July 1966 and operated successfully from launch to termination. The data from the flight shows that in some cases differences in the emission spectra can be detected from balloon altitudes but that interpretation of the data in terms of composition would require a more ambitious program than was warranted in this secondary effort. Such a program would entail ground studies of *in situ* minerals and perhaps ground truth checks

during a flight. As pointed out above the earth presents a difficult problem in this respect and the success of this attempt although limited indicates that such measurements would be meaningful on a body such as Mars.

The results of this experiment were published as Scientific Report No. 1 on this project.[1]

2.2 Balloon Borne Lunar Studies

Prior to the starting date of this contract at the University of Denver, balloon flights intended to record thermal emission spectra of the central portion of the lunar surface were being conducted by AFCRL personnel in conjunction with Dr. A. Howell of Tufts University. The data obtained on these flights indicated that greater sensitivity and better spectral and spacial resolution were needed to discern variations from black body emission in the lunar spectrum.[2] The spectrometer then in use for balloon measurements could not be upgraded to the extent required to significantly improve the measurements, consequently the design and construction of a new spectrometer was undertaken.

It was agreed among project personnel and AFCRL scientists that the improvement which could be obtained by use of a Cu:Ge detector would be sufficient to warrant its use in spite of the restraints on spectrometer configuration and flight operations imposed by the necessity for liquid helium cooling of this detector. A circular variable filter was selected as the spectral element.

With these elements selected a spectrometer compatible with the Tufts University telescope system was designed and constructed by project personnel.

The spectrometer and telescope system were flown for the first time in March 1967. The spectrometer functioned normally and several spectra of the region near the crater Theophilus were obtained before the pointing control ceased to track the moon. The data obtained were

r ·ccd at the University of Denver and published along with some of their ground based observations and a discussion of their significance by Hunt and Salisbury.[3]

Additional data were obtained during subsequent flights and on 12 April 1968 three hours of excellent data were obtained for six areas of the lunar surface. The data from this flight have been reduced. A journal publication is being prepared in conjunction with AFCRL scientists. The data indicate spectral differences between the lunar Maria and areas expected to be composed of highland material. The spectral differences appear in the 7.0μ - 8.5μ region and are apparently connected with the Christianson frequency effect which Conel[4] has shown to occur in silicate powders.

Samples of the spectral emissivity of a region around the crater Copernicus as calculated from the balloon flight data are shown in Figure 1. The spectral emissivity curves shown in Figure 2 were calculated from balloon flight data taken from a region in Mare Serenitatus. Each curve represents approximately twenty co-added spectra. These curves are numbered in chronological order The observations represented by each curve are separated in time by approximately one hour. The curves are successively displaced by 2.5% for the sake of clarity. The large spectral feature centered at 9.6μ is due to atmospheric ozone.

Two additional flights were conducted with the equipment and data obtained on both of them. The areas observed on these two flights include two of the areas previously examined and four areas where data were not taken before. The data from these two flights are currently being reduced. The reduction of this data is being slowed by the loss of the instrumentation on the last of these flights.

2.3 Instrumentation

Four spectral radiometers were constructed under this contract; a grating spectrometer for terrestrial terrain measurements

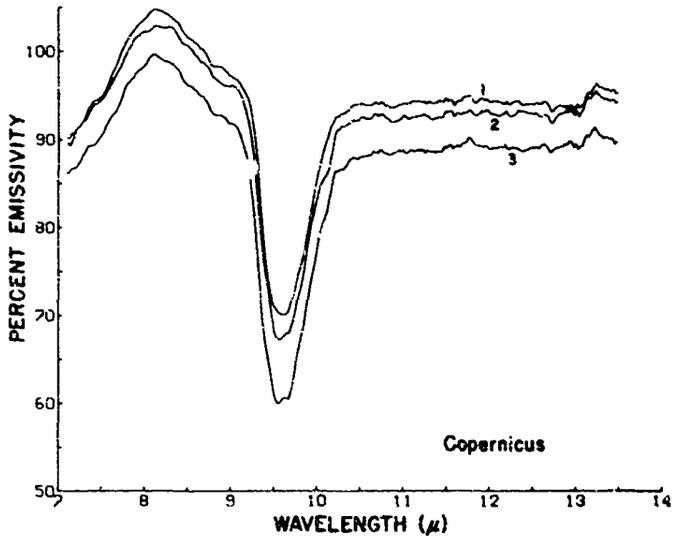

Figure 1. Spectral Emissivity of a Region Around the Crater Copernicus.

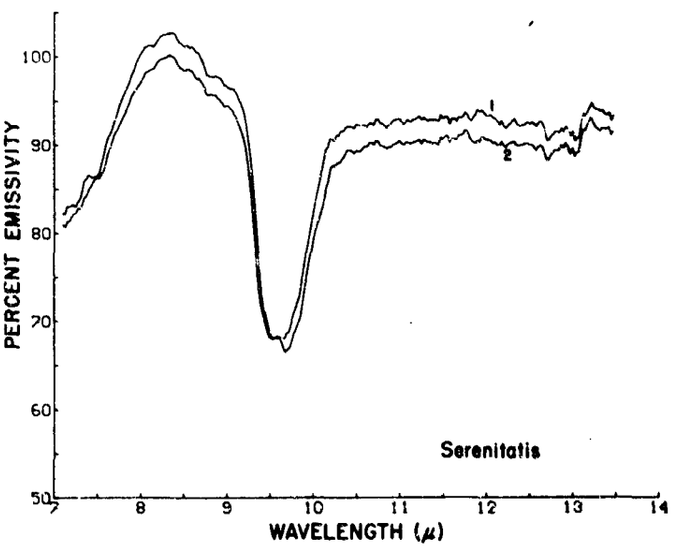

Figure 2. Spectral Emissivity of a Region in Mare Serenitatis.

and three similar circular variable filter instruments for lunar studies and laboratory use.

The grating instrument was of conventional Czerny-Turner design with a focal length of one meter. The grating was a Bausch and Lomb replica grating ruled with 75 lines/mm. A Reeder thermocouple was employed as a detector, and the spectrum was scanned in 2.5 minutes with a resolution of approximately 0.08μ. An off-axis, folded-beam telescope, with a 25 cm aperture and 200 cm focal length, was used as foreoptics to limit the field of view to 2x5 milliradians. The spectrometer with foreoptics was approximately 2 meters long and weighed about 100 pounds.

The three circular variable filter instruments were designed to be as compact and light as possible, since space available for the Lunar spectrometer on the rear of the telescope was limited and the entire spectrograph was pointed along with the primary mirror. The finished instrument weighed 17.7 kilograms and was approximately 60 cm x 25 cm x 20 cm overall.

The scan rate of the spectrometer was variable in 5 steps from 25 seconds per filter wheel rotation to 90 seconds per rotation. A range of 2.5 minutes to 10 minutes could be obtained with the interchange of one gear and drive belt. The spectral resolution was a function of the filter wheel, approximately 2% of the wavelength for the 7.0μ - 14.0μ filter employed in the original instrument and 1% of λ for the 7.5μ- 15μ filters used in the laboratory instrument and the replacement flight instrument. The field of view was determined by an aperture at the filter wheel and could be increased or decreased with different apertures. The aperture utilized for flight gave a field of view of approximately 3 minutes of arc through the telescope optics.

With a 10-minute integration time obtained by coadding the spectral scans a signal-to-noise ratio in excess of 300/1 was obtained for lunar temperature targets with the flight instrument.

With the exception of the filter wheel as mentioned above and minor modifications, the second and third C.V.F. were identical with the original. One was constructed to permit comparison of the lunar data with laboratory spectra run on a similar instrument and the other will replace the original instrument which was lost on a balloon flight.

The reduction of the data recorded on analog tape during the flights was done on a digital computer, thus requiring conversion of the analog data into digital form as a first step in the reduction. In order to eliminate this step and improve the dynamic range of the recording, the recording system was modified to accommodate an on-board digital tape system. This involved building an analog-to-digital conversion unit and the required tape transport. Testing on the unit was not completed in time for its incorporation into the system prior to the October flight. Consequently the modified unit is operational and will be used on future flights.

2.4 Rock Sample Measurements

As a test of the equipment characteristics a few spectra of powdered rock samples were run and reduced. These are being forwarded to AFCRL scientists for comparison with the lunar data.

3. ION BOMBARDMENT APPARATUS FOR LUNAR SURFACE SIMULATION STUDIES

3.1 Introduction

The purpose of the project described in this report was to investigate the interactions between energetic ions and dielectric surfaces in a simulated lunar environment, in an effort to understand some of the effects of solar wind protons on exposed lunar surface materials. For these studies an ion source was required which would produce a beam of protons with the following properties: a flux density substantially greater than the estimated solar proton flux density of 10^8 protons/cm^2 sec, an energy continuously variable between approximately 1 and 20 kev, a small energy spread, and a high degree of purity.

In the first stages of the project two such ion sources were developed, tested, and installed on existing vacuum systems at Air Force Cambridge Research Laboratories. The first of these sources was non-bakeable and was useful only at relatively high pressures, due primarily to the use of O-ring vacuum seals in its construction. In the design of the second source this deficiency was eliminated and both the operating pressure and the quality of the beam were improved. The sources were of the radio-frequency type first described by Thoneman[1] and later developed by Moak, Reese, and Good[2] at Oak Ridge.

Finally, the experience gained during the testing and construction of these first two sources was applied to the design of an ultrahigh vacuum ion bombardment system which was assembled at the University of Denver. This system, with its improved ion source, will be described here. It is based on designs by Barnfield et al.,[3] and McCracken et al.[4]

3.2 Ion Source

The radio-frequency ion source is illustrated schematically in Figure 3. Basically, it consists of a Pyrex discharge tube mounted on a stainless steel flange. Pyrex is used because it is

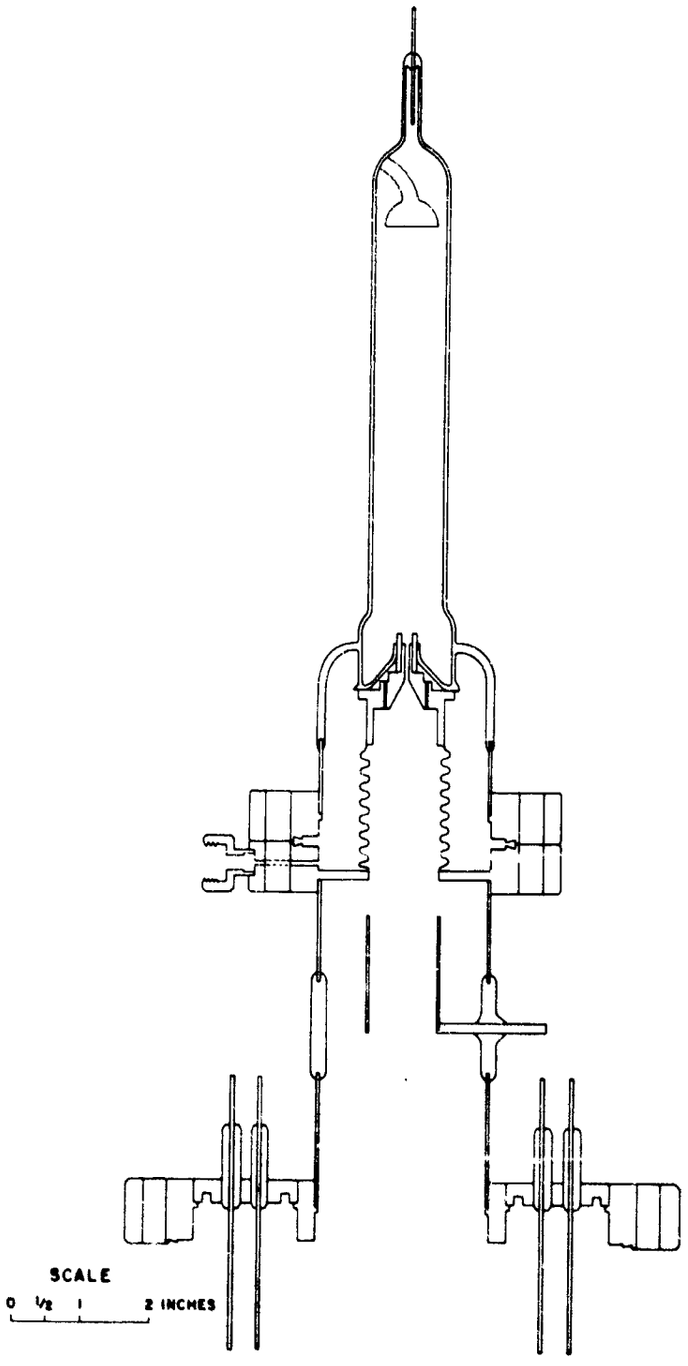

Figure 3 Ion Source

the poorest known catalyst for hydrogen recombination. The discharge tube is a commercially available bottle which has been modified so that it is bakeable. The usual O-ring seals have been replaced by copper gaskets and Kovar-to-glass seals. The unmodified Pyrex tube shown in Figure 4 is sealed directly to a Kovar tube which is in turn welded to a stainless steel flange.

Hydrogen gas is leaked into the bottle through a hole in the side of the flange by means of a variable leak valve. It diffuses in past the small quartz sleeve which surrounds the aluminum exit canal and is pumped out through the canal. The gas in the source bottle at approximately 10^{-2} Torr is ionized by the rf field of an inductively-coupled 30 MHz oscillator. In the vicinity of the exit canal the plasma is confined to the center of the discharge tube by the magnetic field of a solenoid which surrounds the base of the bottle. An electric field applied between the exit canal and the extraction probe at the other end of the bottle then accelerates the protons out through the canal. Electrons are accelerated in the opposite direction and collide with the pyrex shield which protects the tungsten probe.

The canal is 0.076 inch in diameter and 0.5 inch long. It is made of aluminum because aluminum has a small sputtering coefficient. The ground quartz sleeve which surrounds the exit canal serves to hide the metal from the discharge, minimizing surface recombination of the ions. Since the quartz hides the canal, it also functions as a virtual anode when the extraction voltage is applied. Hence the electric lines of force between the static charge built up on the quartz sleeve, and the aluminum exit canal cause the ions to be focussed into the tip of the canal. The aluminum canal screws into a stainless steel housing which is welded to a stainless steel bellows. The bellows is in turn welded to the base flange. The purpose of the bellows is to hold the canal in place against the ground lip on the bottom of the bottle, and to take up the thermal expansion during bakeout. A photograph of the bellows assembly, canal, and ground quartz sleeve is shown in Figure 4.

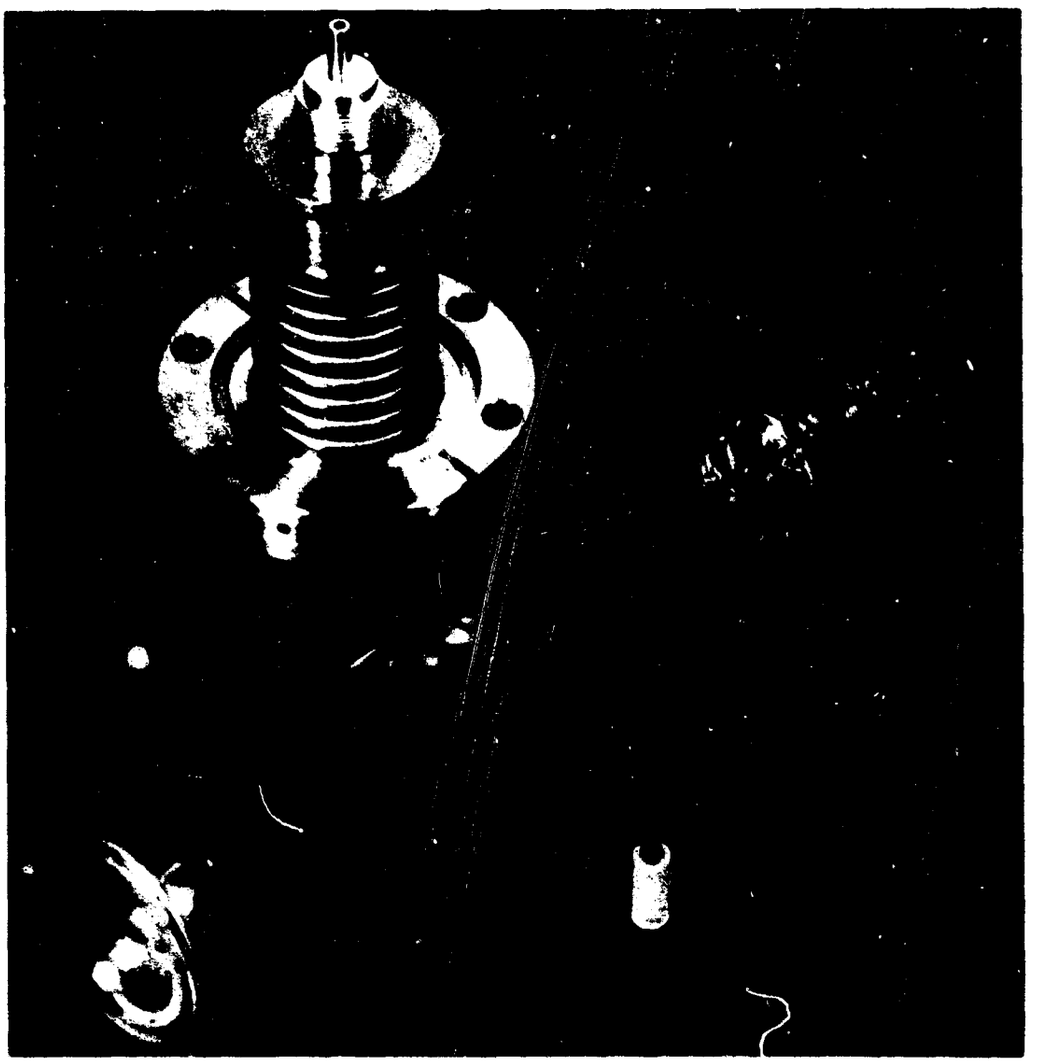

Fig. 2. Ion Source Components

The source can also ionize other gases besides hydrogen, providing beams of heavier ions for comparison with the effects of proton bombardment.

3.3 Vacuum System

Several lunar surface simulation studies have been conducted in vacuum chambers at pressures of 10^{-8} Torr produced by trapped oil-diffusion pumps. Observed changes in surface color, texture, and reflectivity initially attributed to the proton bombardment have been questioned, however, because of unknown interactions between the proton beam and adsorbed gases (a monolayer can form on a clean surface in minutes at 10^{-8} Torr) and the possibility of polymerized hydrocarbon films on the surface from the back-diffusing pump oil.

This system was designed to overcome these objections. No oil or other organic materials were used in its construction, or in any of the vacuum pumps, and the entire system is bakeable. Emphasis was placed upon maintaining a pressure in the low 10^{-10} Torr range in the vicinity of the target surface. At this pressure it would take 10^{4} seconds, or approximately 3 hours, for a monolayer of background gas to form on a clean surface if a sticking coefficient of unity were assumed. Since the rf source operates at about 10^{-2} Torr, it was necessary to design a three-stage differential pumping system to maintain a pressure of 10^{-10} Torr in the target chamber. The vacuum system is shown schematically in Figures 5 and 6. In the first of the three stages, the scattered protons and neutral hydrogen diffusing through the exit canal from the source are pumped by a Granville-Phillips Electro Ion pump, which has a pumping speed of 4800 liters/sec for hydrogen at pressures below 10^{-7} Torr. The pump can hold the chamber pressure in the low 10^{-8} Torr range. As the beam leaves this first chamber it is focussed through a 5mm orifice (with a 10 liter/sec conductance) in order to minimize the diffusion of gas through the magnetic analyzing section. The second stage is pumped by another Electro

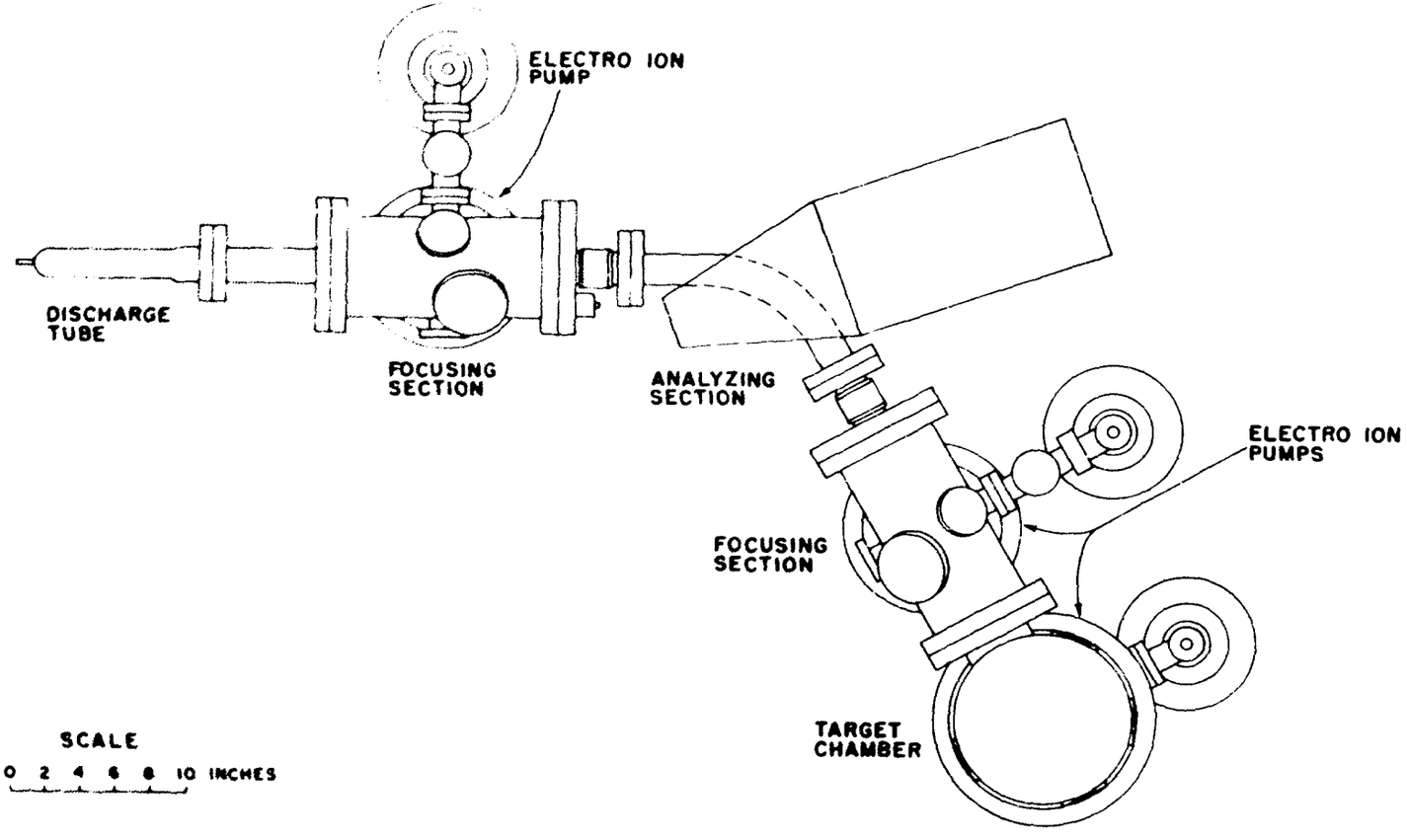

Fig. 5. Ion Bombardment Assembly - Top View

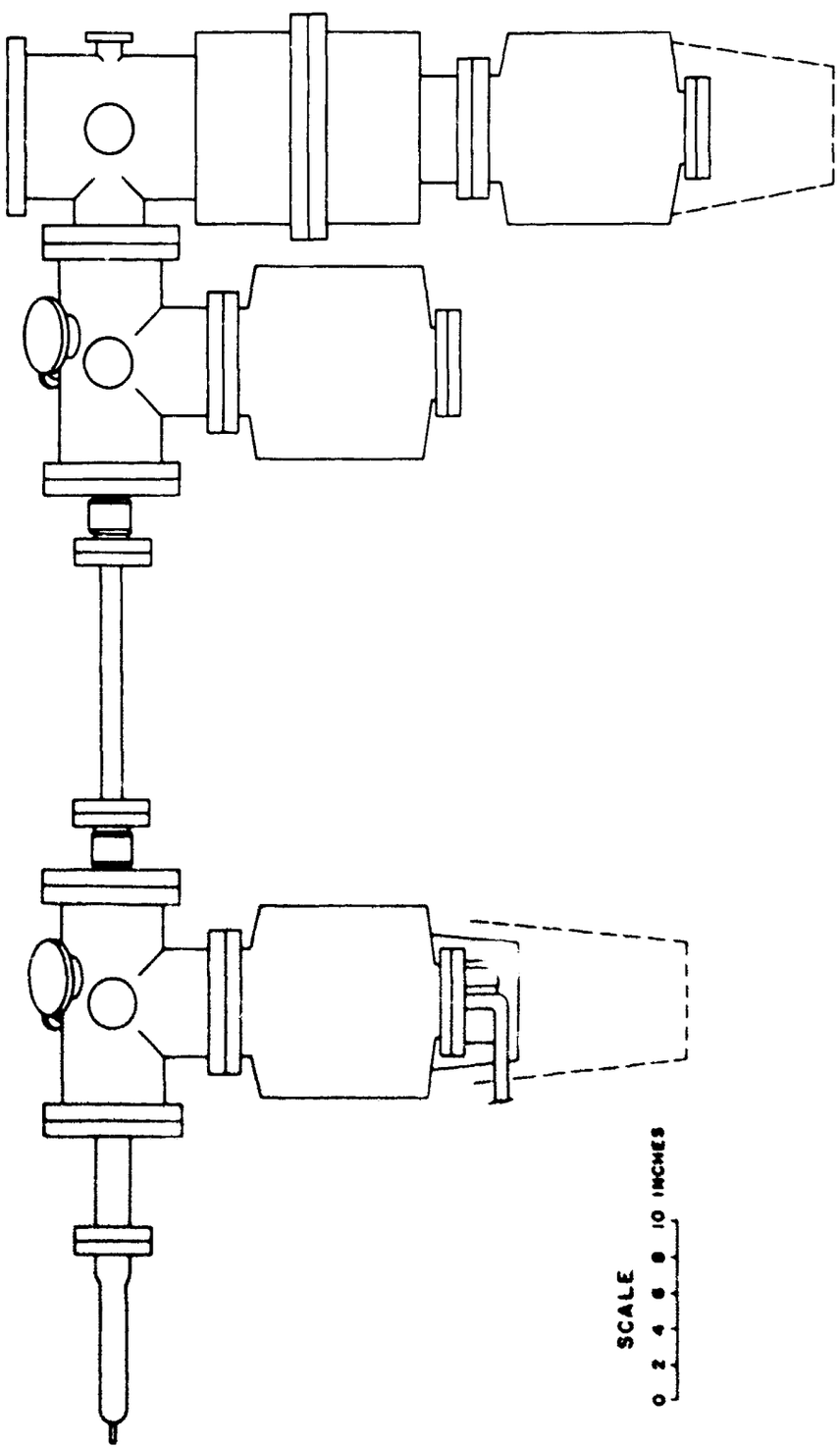

Fig. 6, Ion Bombardment Assembly - Side View

Ion pump which is able to maintain a pressure in the 10^{-9} range. Between the second chamber and the target chamber, the beam is focussed through another 5mm orifice. In the target chamber, hydrogen from the proton beam and gas from the sample are pumped away by a third Electro Ion pump, plus an auxiliary sublimation pump with a liquid nitrogen cooled wall. A 20 microamp proton beam produces 20,000 liters/sec of hydrogen gas in the target chamber. Thus, the combined pumping speed of 30,000 liters/sec for the two pumps will hold the chamber in the low 10^{-10} Torr range with the beam off and in the high end of that range with the beam on. When the system is pumped down from atmospheric pressure, four Varian liquid nitrogen cooled sorption pumps are utilized down to 2×10^{-3} Torr, where the Electro Ion pumps are turned on. Thus no rotary or oil diffusion pumps are used.

3.4 Ion Optical System

After passing through the exit canal, which rides at a high potential, the beam is focussed and accelerated to ground in two stages by consecutive two-cylinder lenses. Two stages are used because at high beam energies the focal length of a single lens is too small. Since the focal length of the accelerating lens system changes with changing beam energy, an Einzel lens[5,6] in the first chamber is employed to focus the beam through the 5mm orifice which separates this chamber from the magnetic analyzing section. Following the Einzel lens there are electrostatic deflection plates to allow for corrections of inaccuracies in mechanical alignment of the various components of the ion optical system.

Next the beam enters a sector magnetic field, by means of which ions of a particular mass may be selected and separated from the rest of the beam. Although the system was designed primarily for protons, the sector magnet is capable of handling 20 keV ions up to mass 20. Hence heavier ions may be compared to protons in their effect upon and interaction with the target surface, thus

contributing to the understanding of the mechanisms involved. Since the beam diverges as it enters the magnetic field, the fringing fields of the magnet are used to obtain vertical focussing at the same point as that of the horizontal focussing produced by the whole field. In this way, the transmission of the analyzing section is increased over what it would be if only the usual horizontal focussing were employed. Fewer ions are lost in collisions with the walls of the analyzer tube. The design of the magnet was based on the theory developed by Camac[7] and Cross.[8] The double-focussing effect is produced by requiring the beam to enter the magnetic field at an angle with respect to the normal of the pole face boundary. The magnet is a 30° sector which will produce a field of up to 5000 Gauss, and the beam is bent through an angle of 60° (see Figure 3). The magnet is mounted on a track and can be withdrawn during bakeout.

Because of the large magnification of the magnetic focussing arrangement, a strong-focussing quadrupole lens pair[9,10] was employed to focus the beam through the second 5mm orifice and onto the target surface at the center of the target chamber. A photograph of the entire system is shown in Figure 7.

3.5 Target Chamber

The target chamber is constructed from an eleven inch stainless steel tube, eight inches in diameter, with a beam inlet port and four sampling ports at 60, 90, 120, and 180 degrees. The sampling ports are used for the mounting of various types of detectors, including a Granville-Phillips rf quadrupole residual gas analyzer, a McPherson photoelectric spectrophotometer for luminescence measurements, and energetic particle detectors for counting both charged and neutral reaction products. The top of the target chamber is a ten inch flange, on which a target positioning turret, a nude ion gauge, and the necessary electrical feedthroughs are mounted. The target positioning turret can be rotated through 360°, and can be translated along the vertical axis perpendicular to the beam. The turret can be used to mount several samples at once, so that the system need not be opened

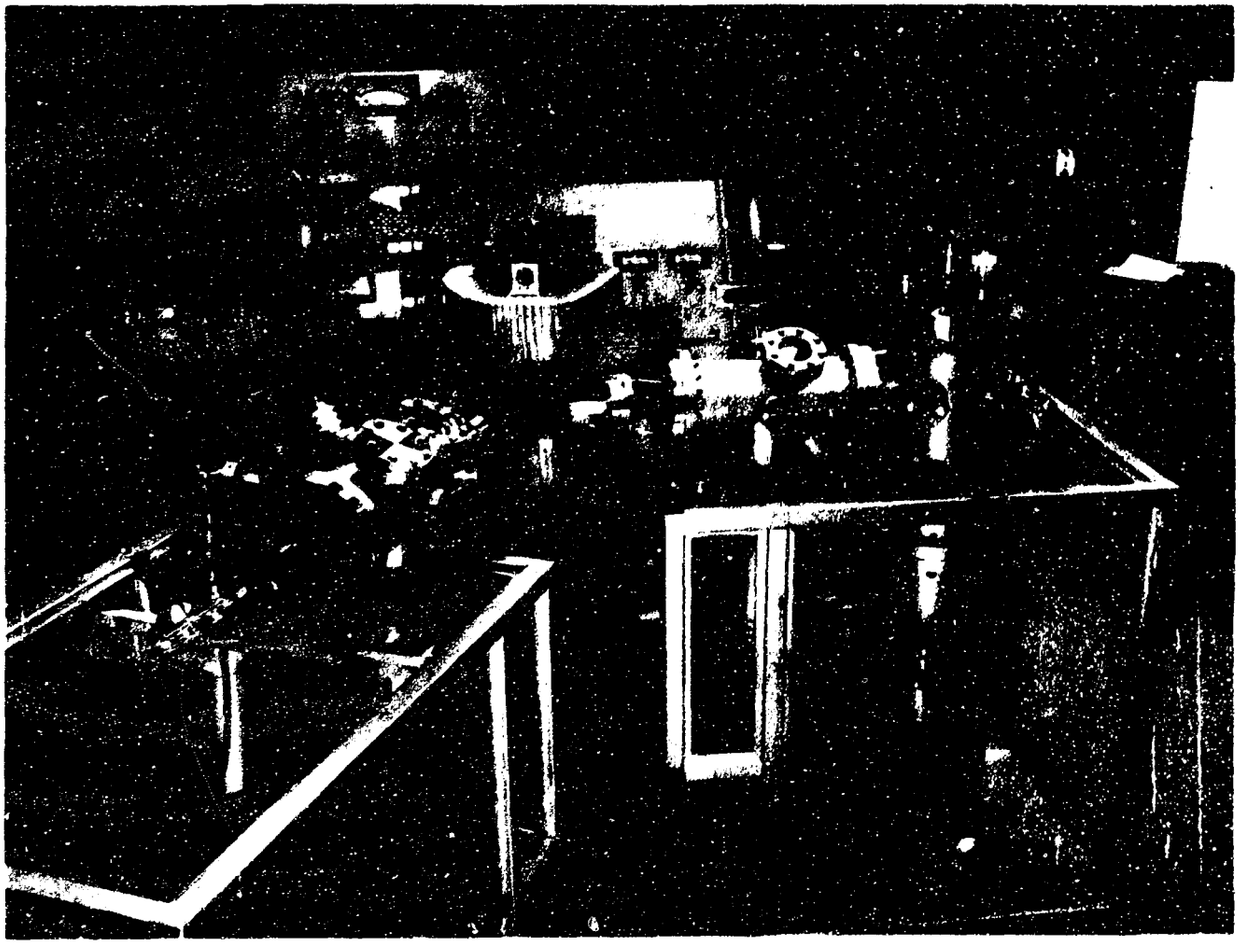

Fig. 5. Ion Bombardment Apparatus

to atmospheric pressure every time a new sample is to be investigated. One position on the turret is generally occupied by a Faraday cup for measuring the beam current. Provision is also made for the mounting of heating and neutralizing filaments, various electrodes for secondary electron suppression, etc., depending upon the particular experiment to be performed. The turret is mounted on a molybdenum shaft which turns and slides in boron nitride bearings. Boron nitride is used because it has an extremely low coefficient of friction, even in a very high vacuum, and because it can be baked and has good vacuum properties. Molybdenum is used because it has a coefficient of expansion close to that of the boron nitride.

3.6 Improved Ionizer for Neutral-Particle Detection

Surfaces subjected to ion bombardment emit neutral and charged particles arising from (a) reflected beam ions; (b) surface-neutralized beam ions; (c) desorbed species from the surface-adsorbed layers; (d) sputtering of the crystalline surface. The largest neutral component is presumably that due to neutralized beam particles, which will be fast hydrogen atoms under proton bombardment. The neutral flux arising from desorption will be time-dependent under conditions in which the flux of ions in the beam greatly exceeds the flux of background gas to the surface. For a beam current of 10 microamperes on one cm^2 of surface in an environment of 10^{-10} Torr background gas pressure, collisions of the proton with the surface are about 10^3 more frequent than for the background gas molecules. Under this condition, desorption of surface-adsorbed species can be readily achieved provided that the desorption efficiency ϵ_d (which should be greater than the sputtering efficiency) for protons is greater than 10^{-3}. A value of $\epsilon_d = 0.1$ would permit the removal of a monolayer of adsorbed gas in about five minutes. It is of interest, therefore, to monitor the desorption rate of the various chemical species with time, as well as the flux of sputtered particles. For light ions, the sputtering efficiency might be expected to be quite dependent upon surface cleanliness.

In order to improve our capacity to observe the neutral flux of particles arising from the surface, we designed a neutral-particle ionizer which is expected to have a much higher efficiency than the typical ionizer supplied on commercial residual-gas analyzers. Briefly described, the ionizer employs a circular loop of tungsten filament wire, through which the neutral beam may pass. The filament is surrounded by a repeller designed to force the electrons to the center of the beam. A solenoid is used to sweep the electrons along the beam axis, thus increasing by a large factor the mean interaction length for the electrons and beam particles. Preliminary tests have shown that for 15 ma of electron emission current, an ion current of 500 ma/Torr could be attained. However, because of the solenoid, the ionizer was not bakeable and was therefore not employed in the experiments described in the next section. The very high sensitivity of the ionizer could be duplicated, however, in a bakeable version.

3.7 Experimental Results: Luminescence

There is some evidence that part of the light which we receive from the moon, both in general over the entire surface of the moon and during certain localized enhancement events, is due to luminescence of the surface, excited by high-energy radiation from the sun. In the present project, a few preliminary experiments have been performed in an attempt to simulate this lunar luminescence in the laboratory for solar-wind type protons. In these studies single crystal quartz has been bombarded by 2-10 ons and other ions and the resulting optical emission spectrum has been measured. If a solar proton current density at the lunar surface of 10^8 protons/cm^2 sec is assumed, then a proton beam of 10 microamps focussed on an area of 0.1 cm^2 on the sample surface would be equivalent to approximately a year of lunar exposure per second.

The McPherson photoelectric spectrophotometer, mounted on one of the four observation ports on the side of the target chamber, was used to measure the emission from the quartz sample inside the

chamber. A sample luminescence measurement, made while the target was being bombarded by a 7 keV proton beam of only 2 microamps, is shown in Figure 8. The luminescence is blue in color and is strong enough to be seen quite easily with the naked eye. Intensity is given in arbitrary units in the figure. It should be noted that the spectrum has not yet been corrected for detector response.

Similar experiments have been done using both H_2^+ and N^+ ions, with the same quartz crystal. In the case of the H_2^+ ions the luminescence spectrum is identical to that of the protons, but in the case of N^+ there are some differences. The nitrogen ions excite the same broad band spectrum of luminescence as the protons and H_2^+, except that in addition a few narrow peaks (roughtly 20 Angstroms in width) appear superimposed on the original curve. Three of these peaks have been observed, at approximately 5063, 5800, and 5925 Angstroms. It is interesting that while all three of these peaks appear at an incident ion energy of 9 keV, only the third one appears if the energy is lowered to 5 keV. Measurements of the exact threshold energies for these three peaks have yet to be made. Also, it is possible that other new peaks may appear at even higher energies. None of them have as yet been identified with any particular molecular or atomic transitions.

Another effect which has been observed is a change of intensity with time. In the case of nitrogen ion bombardment at 7 keV the height of the peak shown in Figure 8 falls off to half of its original value after two hours of continuous bombardment. If the sample is then brought up to atmospheric pressure for 24 hours and then pumped back down and bombarded again with 7 keV ions, the intensity of the luminescence shows no recovery whatsoever. Hence the drop in intensity is attributed to destruction of the crystal lattice rather than either a charging up of the sample or a desorption of gas layers from the surface. The narrow peaks mentioned in the previous paragraph show the same effect. However, it is interesting to note that the heights of all of the peaks (including the broad peak in Figure 8) can be made to recover by simply

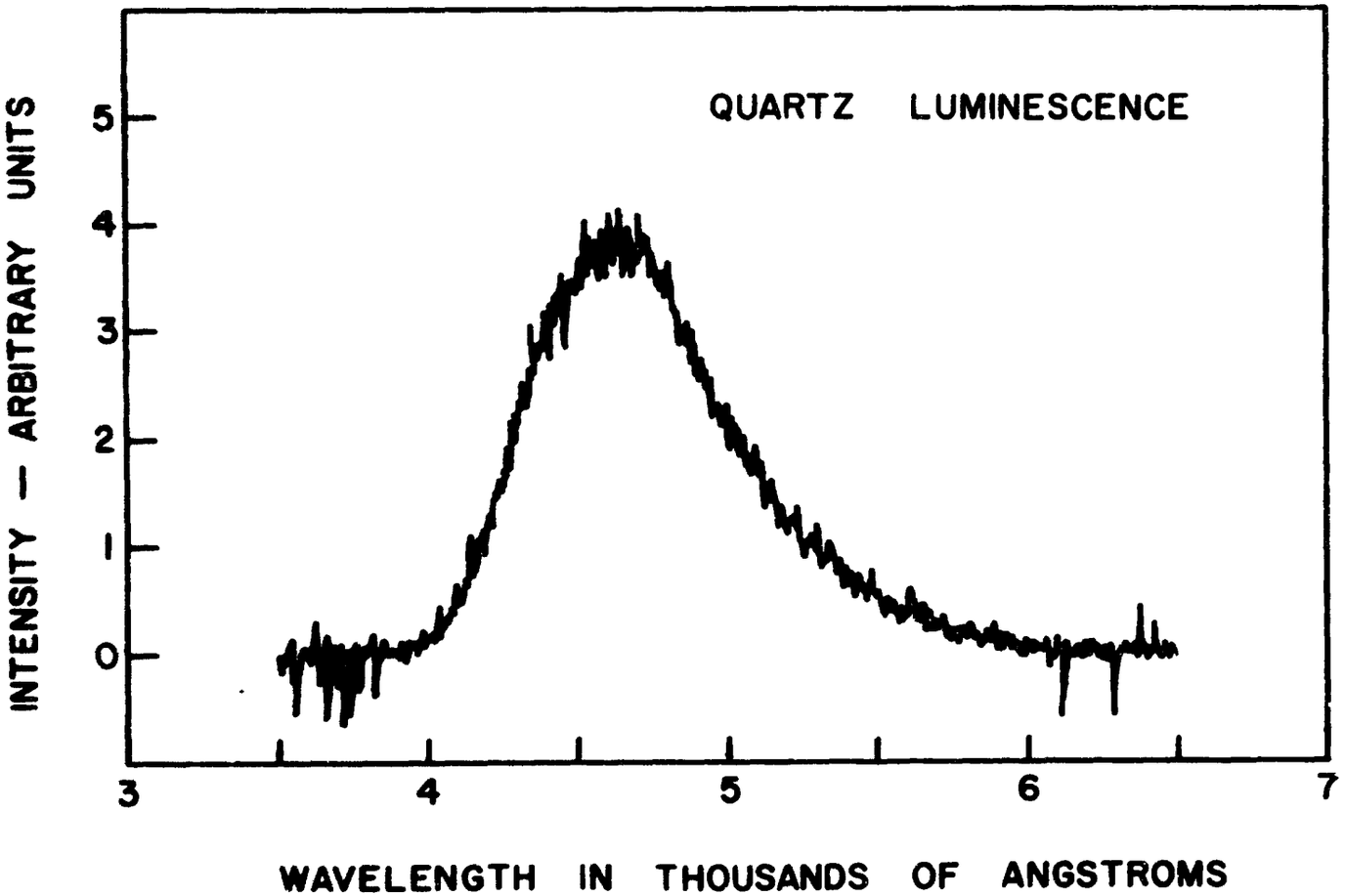

Figure 8. Quartz Luminescence Excited by 7 keV Protons

increasing the incident ion energy. This effect may probably be attributed to the fact that the ions reach deeper into the crystal lattice when they have greater energies.

There are of course changes in luminescent intensity with varying ion energy and current density, but in all of the cases studied so far the change in intensity appears to be uniform over the entire frequency range. The variations of intensity with ion current and with ion energy have not yet been studied quantitatively.

4. SINTERING STUDIES

4.1 Problem Definition

Since a state of aggregation and consolidation of the lunar surface is not presently known, it was desired to obtain fundamental information concerning these conditions.

This information is required for lunar exploration and lunar technology development, and could contribute to possible hypotheses concerning the origin and age of the moon. Thermal inertial and angular reflectivity data point to a lunar-surface outer layer of dust or powder. More recent observations via Surveyor III indicate that the consistency of this outer layer of dust is similar to that of wet sand. Immediately beneath this outer layer of "wet sand" there seems to be a harder crust. This study was concerned with the consolidation and formation of the hard crust.

The scientific objective of this investigation was to determine the sintering characteristics of a prototype lunar material. Sintering rates, the sintering mechanism, and the activation energy for sintering are required to adequately describe the sintering characteristics of a particular material. In the present investigation the sintering of olivine basalt was characterized. Very little information is available in the current literature regarding the sintering of olivine basalt. Of the two studies found, neither was concerned with fundamental sintering characterization. Finally, some hypotheses were made regarding the relation of olivine-basalt sintering to theories of the formation of the moon.

4.2 Scope

The scope of the present investigation was quite broad. A postulated lunar material was selected and its sintering characteristics determined. Since the selected prototype material was a silicate, it was likely that it would exhibit some sintering characteristics typical of glasses. Hence, viscous-flow sintering theory was reformulated in an effort to allow more precise sintering characterization of the postulated material. The reformulated

theory was experimentally verified. The relationship between the sintering of vitreous and nonvitreous materials was examined. Finally, attempts were made to extrapolate the sintering characteristics of the postulated material to lunar thermal conditions, and hypotheses were made concerning the degree of sintering of the lunar surface and the history of the moon.

Olivine basalt has sufficient silica content to be a good glass-former. Many studies of the thermal history of the moon indicate that there was indeed enough heat at one time to cause a silicate such as olivine basalt to be vitreous for a period of time. Therefore viscous-flow sintering was expected to play a major role in the sintering characterization of lunar olivine basalt.

Because the sintering characterization of olivine basalt had to be as precise as possible for extrapolation to lunar thermal conditions, viscous-flow sintering theory was examined and subsequently reformulated. More accurate approximations of the geometric models were introduced resulting in new and more illustrative theoretical equations for viscous-flow sintering.

A portion of the present study was devoted to the experimental verification of the reformulated viscous-flow theory. The material selected for these validation experiments was a well characterized single-phase, sodium-borosilicate glass. The verification of the new theory was based on analyses of the mechanisms, activation energies, and necking curvatures for the sintering of sodium-borosilicate glass spheres.

The sintering of olivine basalt was characterized by studying the sintering behavior of three forms of olivine basalt. Polycrystalline olivine-basalt powder compacts, vitreous olivine-basalt spheres, and devitrified olivine-basalt spheres were used in the sintering characterization. The sintering mechanism was deduced from experimentally determined sintering rates and from microstructural considerations.

Finally, making assumptions regarding the rate-controlling process and using the experimentally determined sintering characteristics of a typical silicate (olivine basalt), extrapolations were made to lunar thermal conditions by means of activation energy considerations. From these extrapolations hypotheses and speculations were made concerning the length of time required for lunar dust consolidation and aggregation, the mode of formation of the moon, the possible explanation of the rays, and the age of the moon.

4.3 Experimental Procedures

Several experimental procedures were used in this study of the sintering of some silicate materials. The silicate materials which were studied are Owens-Illinois KG-33 glass spheres, vitreous olivine-basalt spheres, devitrified olivine-basalt spheres, and polycrystalline olivine-basalt powder. The experimental procedures involved range from preparation of the olivine-basalt spheres and their characterization to the sintering measurements and microscopic examination of sintered bodies. Detailed results and their interpretation are discussed in a Ph.D. thesis now being prepared by Weldon Schaefer.

4.4 Conclusions

The following are the conclusions arising from this research investigation.

1. Viscous-flow sintering theory as originally developed by Frenkel has been reformulated. In the present analysis, an average radial shrinkage was applied rather than the previously used maximum radial shrinkage. In addition, more accurate approximations of the geometry of the twin-sphere and twin-cylinder models were incorporated. Relations between linear shrinkage, necking curvature, surface-area reduction, and necking angles were obtained. The necking curvature was shown to be independent of surface tension and viscosity. Calculated curves were presented to predict the theoretical behavior of necking curvatures.

2. The reformulated viscous-flow sintering theory was experimentally validated by sintering experiments with sodium-borosilicate (Owens-Illinois KG-33) glass spheres. The experimental measurements of neck-growth and shrinkage rates were found to correspond to those for viscous-flow sintering. The measured necking curvatures were observed to be consistent with the reformulated viscous-flow sintering theory. Viscosity values for KG-33 glass at various temperatures were calculated from the sintering data and found to agree with the viscosity values furnished by the supplier. The activation energy for the viscous-flow sintering of KG-33 glass spheres was calculated from the viscosity values at various temperatures to be approximately 62 kcal/mole.

3. Unusual sintering behavior was observed for vitreous olivine-basalt spheres. The shrinkage and neck-growth rates could not be ascribed to any particular sintering mechanism. The necking curvatures could not be correlated with the theoretical curvatures predicted by the reformulated viscous-flow theory.

4. The rapid initial shrinkage observed for the sintering of compacts of devitrified olivine-basalt spheres was interpreted as a simple rearrangement facilitated by the presence of a liquid phase. Electron probe micro-analysis of sintered specimens of devitrified olivine-basalt spheres shows the presence of a liquid phase containing iron and calcium.

5. The shrinkage rates for olivine-basalt powder compacts could not be interpreted in terms of the usual solid-state sintering mechanisms. Shrinkage was observed only in a narrow (30-40°C) temperature range; the slopes of the shrinkage-rate curves ranged from 0.13 to 0.24. However, the shapes of the shrinkage curves for the sintering of olivine-basalt powder compacts were similar to those previously observed and attributed to sintering in the presence of a liquid phase by other authors. The observed microstructures were characteristic of sintering in the presence of a

liquid phase. In addition, the electron probe microanalyses of the sintered compacts of polycrystalline olivine basalt yielded evidence for the presence of a liquid phase containing iron, silicon, and calcium. Previously reported phase equilibria studies show the possibility of formation of a liquid phase at the temperatures employed in sintering experiments of this investigation.

6. By making assumptions concerning the rate-controlling processes occurring in the sintering of olivine basalt, speculations and hypotheses were made concerning the role of sintering in the aggregation and consolidation of the lunar surface.

5. SURFACE PROPERTIES

5.1 Introduction and Statement of Problem

The purpose of this study was to obtain some information about the behavior of surfaces in a simulated lunar environment. In particular we addressed ourselves to the problem of assessing whether or not and to what extent cracks in silicate materials which are produced by loading in a high vacuum, will reheal when the load is released.

This would complement the work of Ryan[1] who studied the adhesion of polished flat silicate surfaces in vacuums to 10^{-12} Torr, but would be more closely related to the failure mode of these materials in a lunar environment.

Two approaches were considered for this study. The first was to try to produce a crack in a specimen, which was completely internal. In this manner, the atmosphere would never be admitted to the crack to contaminate it. The load producing the crack could then be cycled to determine to what extent rehealing was taking place from the hysteresis. The second was to build an apparatus which would perform a cleavage test with an Obreimoff-Gilman type specimen in a vacuum of 10^{-11} - 10^{-12} Torr, and obtain a measure of the rehealing from the work to refracture a given area of crack.

It was decided to attempt the first approach which appeared easier and did not require the construction of some fairly elaborate and expensive equipment. This was a mistake. The second approach was tried only after it became apparent that the first would not work.

5.2 Internal Crack Method

Several methods for producing internal cracks were tried.

5.2.1 Crack Initiator Methods

The first of these consisted of a single-leaf bellows type

of initiator Figure 9. Since the material selected for study was pyrex glass, the initiator was manufactured from Kovar and a cylindrical glass specimen was cast around it. A high frequency induction furnace was modified to accomplish the casting process.

In order to initiate a crack, hydraulic pressure was introduced into the bellows causing it to expand and initiate a crack at the periphery. A hydraulic system (Figure 10) was assembled for this purpose. Three such specimens were prepared and tested. In all cases a crack initiated internally at the periphery of the bellows and propagated rapidly to the outside surface of the glass. The crack was always coplanar with the bellows, but could not be stopped prior to reaching the outer surface even when incremental loading was used. It was evident that the loading system was to "soft".

Consequently the crack initiator was redesigned to a double ended configuration which could be loaded in a tensile machine. A ring was added to the outside edge of the glass specimen to supply a compressive stress and prevent the crack from propagating to the edge (Figure 11). When this configuration was tested, the crack initiated as before, i.e. in the plane of the bellows, but rapidly deviated from this plane until it arrived at the top surface of the specimen. Initial tests with this configuration were made using a brass bellows and a glassy polymer (polyester resin) for the specimen. These were much less expensive to fabricate and allowed us to vary specimen dimensions easily. We were occasionally able to arrest a crack in a polyester sample, but were unable to do so with glass.

5.2.2 Stress Initiation by Radial Compression

A second stress initiation method that was tried, used a modification of the diametral compression or Brazil test.

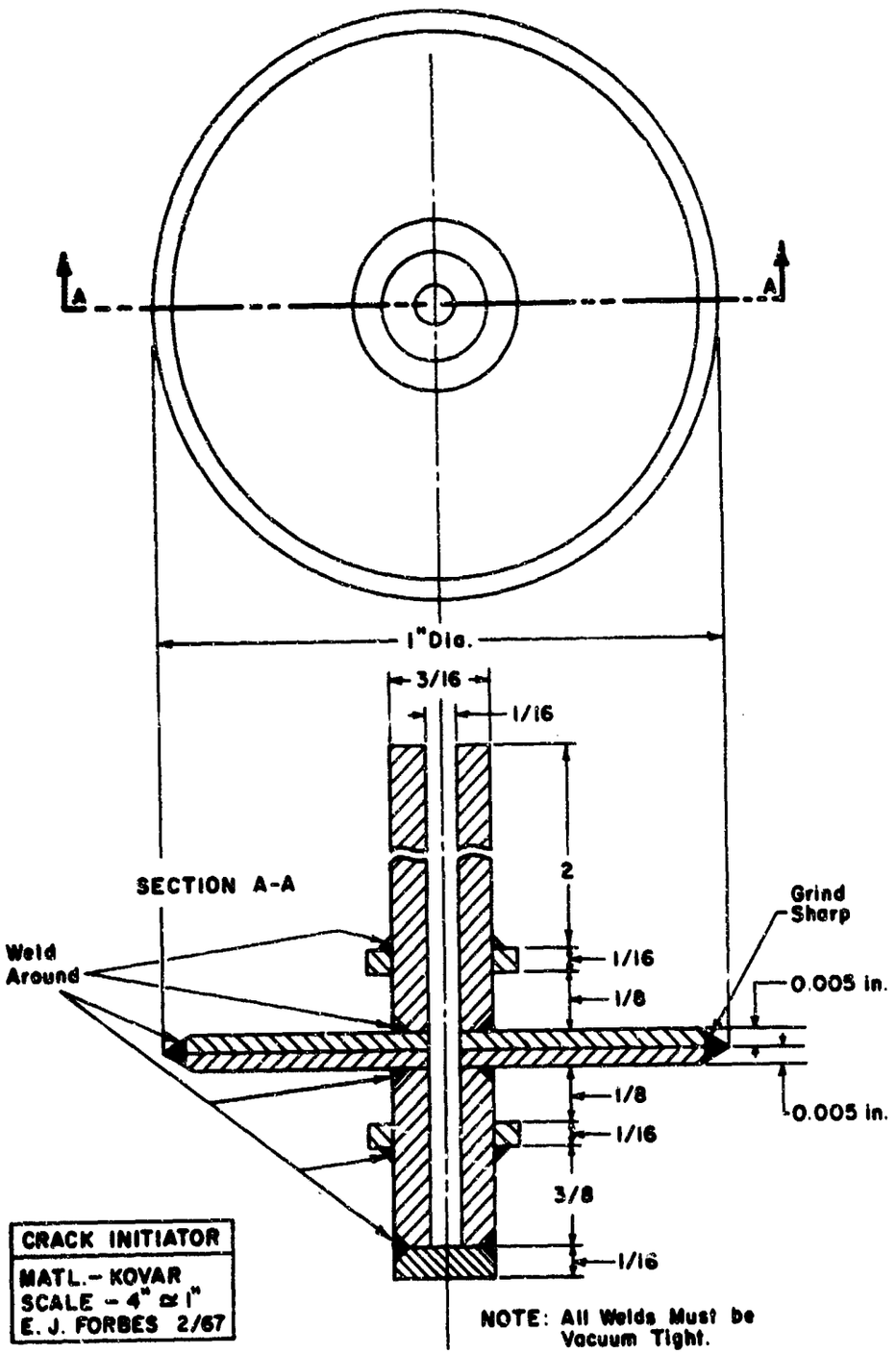

Figure 9. Kovar Crack Initiator.

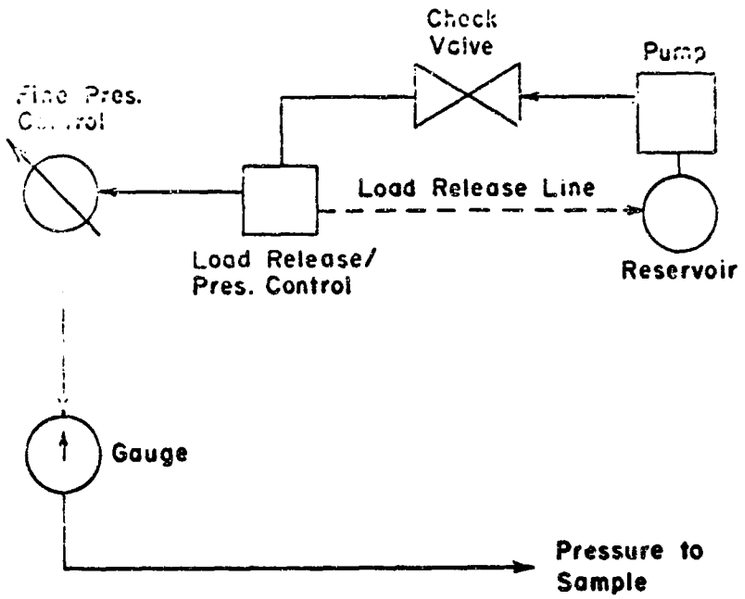

Figure 10. Schematic Diagram of Hydraulic System

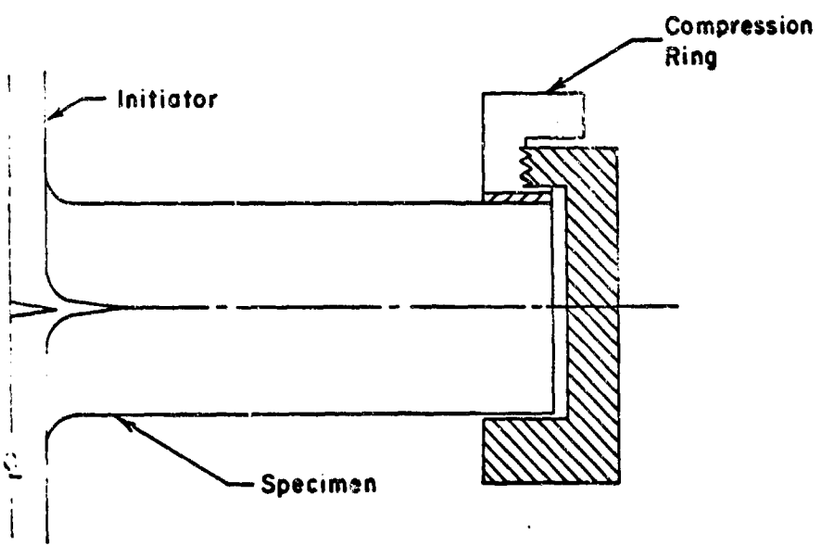

Figure 11. Modified Kovar Initiator

The Brazil method consists in compressing a cylinder diametrally between two flat plattens at opposite ends of a diameter AB (Figure 12).

It can be shown theoretically that there exists a principal tensile stress σ_{xx} of constant magnitude along AB given by:[2]

$$\sigma_{xx} = \frac{2W}{tD} \tag{1}$$

where W = applied load, t and D = thickness and diameter of the cylinder, respectively.

A second compressive principal stress σ_{yy} is given by:

$$\sigma_{yy} = -\frac{2W}{\pi t}\left[\frac{2}{D-2y} + \frac{2}{D+2y} - \frac{1}{D}\right] \tag{2}$$

and varies from a maximum at A and B to a minimum, equal to $-3\sigma_{yy}$ at O. In tests with brittle materials specimens are frequently observed to fail in tension across the plane AB with the crack not proceeding completely to A or B. Furthermore the failure mode does <u>not</u> depend on the thickness (t) of the cyliner particularly with thin discs ($t<D/10$). Thus for thin discs, W approaches a point load. If a second disc is now added, perpendicular to the first, (Figure 13), there will be two equal principal tensile stresses σ_{xx} and σ_{zz} of magnitude $W/\pi tD$ along AB as well as σ_{yy}. If the discs are now considered as elements of a sphere compressively loaded along a circumference in the x-y plane, (Figure 14) the state of stress for an element at the sphere center is easily obtained by superposition. It consists of a principal tensile stress $\sigma_{zz} = \frac{2W}{\pi tD}$ tending to pull the sphere apart at the x-y plane and principal compressive stresses $\sigma_{xx} = \sigma_{yy} = -2.5\sigma_{zz}$. With increasing radial distance from the center and in the x-y plane, σ_{zz} decreases to $\frac{W}{\pi tD}$ near the sphere edge, while σ_{xx} and σ_{yy} increase approximately as in the Brazil test.

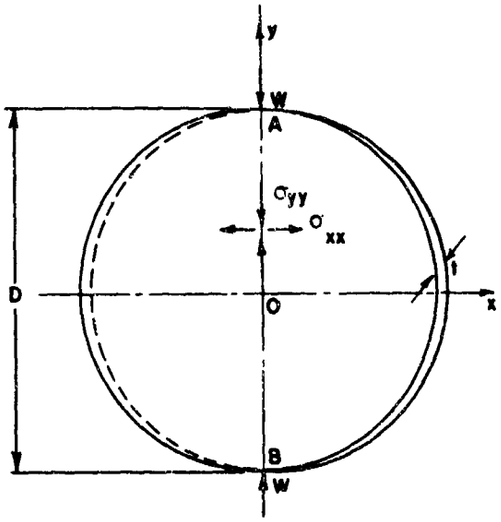

Figure 12. Brazil Test.

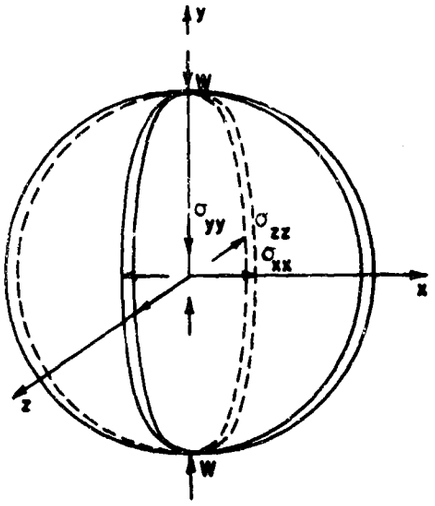

Figure 13. Diametral Compression of Two Orthogonal Discs.

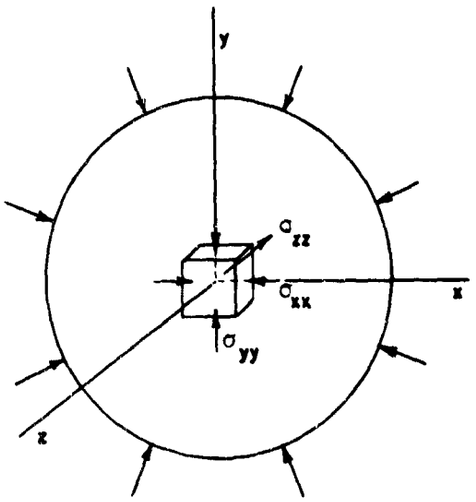

Figure 14. Circumferential Compression of a Sphere.

Thus a spherical specimen geometry loaded as shown in Figure 14 concentrates the tensile stress at the center of the sphere across the x-y plane where a stress concentrator can be placed to initiate an internal crack. The stress state would tend to stop the crack before it reaches the circumference even more effectively than the Brazil test.

The above solutions are not rigorous since singularities are introduced at the loading circle. A more accurate though more complex solution can be obtained by superposition of the classical solution of Sternberg and Rosenthal[3] for diametral point loading of an elastic sphere.

Spherical, polymer and pyrex samples were prepared containing stress initiators in the form of 1/8" x .020" discs of nickel for the polymer specimens and of Kovar for the pyrex.

A simple and effective way of line loading the spheres in compression along a circumference turned out to be as follows. The sphere was placed in a steel split ring of the same diameter and having a contact area width 1/8 the sphere diameter or less. A compressive load was then applied to the ring (whose outer edges are square) by a tensile testing machine.

The results obtained confirmed our semi-quantitative estimates that the sphere would fail in tension across the diametral loading plane. This was found to be the case particularly with the polymer specimens, for which the diametral loading plane was made to coincide with the plane of the initiator disc. As before, it was occasionally possible to arrest the crack with a polyester sample but not with pyrex samples.

Several other specimen geometries and loading methods were tried since the polymer samples were easily fabricated. None of these gave the desired result. It was therefore decided to pursue the alternative plan of conducting cleavage experiments at high vacuum (10^{-11} to 10^{-12} Torr).

5.3 Cleavage at High Vacuum

These experiments would differ from those of Ryan et al.,[1] in that the extent of rehealing of a cleavage crack can be studied at short times after its formation, rather than the adhesion after complete cleavage. In addition it occurred to us that the necessary apparatus, with minor modifications is very well suited to the study of fatigue crack propagation in high vacuum.

Fatigue mechanisms may play an important role in the fragmentation of rocks in a lunar environment to form a "soil". The required reciprocating stresses are provided by the impact of small meteorites and ejected fragments from larger meteorites. These may act somewhat like sand or shot blasting which is well known to produce highly deformed and ultimately fatigue fractured surfaces on metals. In addition, thermal stresses may be significant in larger ejected blocks as evidenced by exfoliation of large granite boulders in East Africa. Fatigue studies in vacuum are rather rare, even with metals, but a recent finding by Regis Pelloux[4] at Boeing has shown a pronounced decrease in crack propagation rate and surface roughness in aluminum at vacuums as low as 10^{-3} to 10^{-4} Torr. Although fatigue of silicates in air has not warranted much study, fatigue in high vacuum may be an important fracture mechanism, in view of the large adhesive forces measured by Ryan particularly at short times after cleavage.

The equipment required for these experiments consisted of a vacuum system and chamber having a low force, or a compensated mechanical feed-through. Cleavage specimens were of the double cantilever, Obreimoff-Gilman type. Such a system has been built and successfully operated by Gordon E. Gross of Midwest Research, for determining cleavage energy of ionic crystals.[5] We contacted Dr. Gross and he very kindly gave us information on design, construction, suppliers and debugging. We made the following minor modifications to Dr. Gross's design. 1) Larger vacuum chamber to permit longer tests. 2) Window port at the side of vacuum chamber

to allow monitoring of crack propagation. 3) Location of both roughing and high vacuum pump on one end of the vacuum chamber to permit heater and thermocouple feed-throughs, easier specimen insertion, and possible future attachment of a proton source.

A vacuum of 11-12 scale (10^{-11} to 10^{-12} Torr) was provided by a 140 l/s vacion pump with cryogenic (L-N) and titanium sublimator auxiliaries, recommended by Varian. Modified stock Varian parts composed the remainder of the system. A schematic of the specimen chamber is shown in Figures 15 and 16.

All components were mounted on an aluminum channel which was attached to the crosshead of an Instron testing machine. The Instrom was equipped to supply the desired types of loading and to record stress and displacement. Crack propagation could be followed microscopically, through the viewing port. The assembled system is shown in Figure 17.

The specimen chamber (Figure 18) accommodates the Obriemoff-Gilman type cleavage specimens (Figure 19) and is fitted with a low force mechanical feed-through and a viewing port. The cleavage force is applied to the specimen through a 3 fingered yoke. The central finger is attached to the specimen after passing through the horizontal bellows, while the two outer fingers are attached to the load cell of an Instron mechanical testing machine. In order to perform an experiment a specimen is placed in the chamber, the desired vacuum pulled on it after which the specimen chamber (with vacuum system attached) is bolted to the crosshead of the Instron. The cantilever action of the rather heavy vacuum system is almost exactly balanced by an automatically controlled hydraulic system (box beneath crosshead) built earlier in the project for a different purpose. This arrangement allows easy and rapid attachment and removal of the system from the Instron as well as easy calibration. The alternative arrangement of attaching the system upside-down to the upper crosshead is considerably more cumbersome.

Our first few runs with the vacuum system revealed a problem with the titanium sublimator which is being taken care of by Varian.

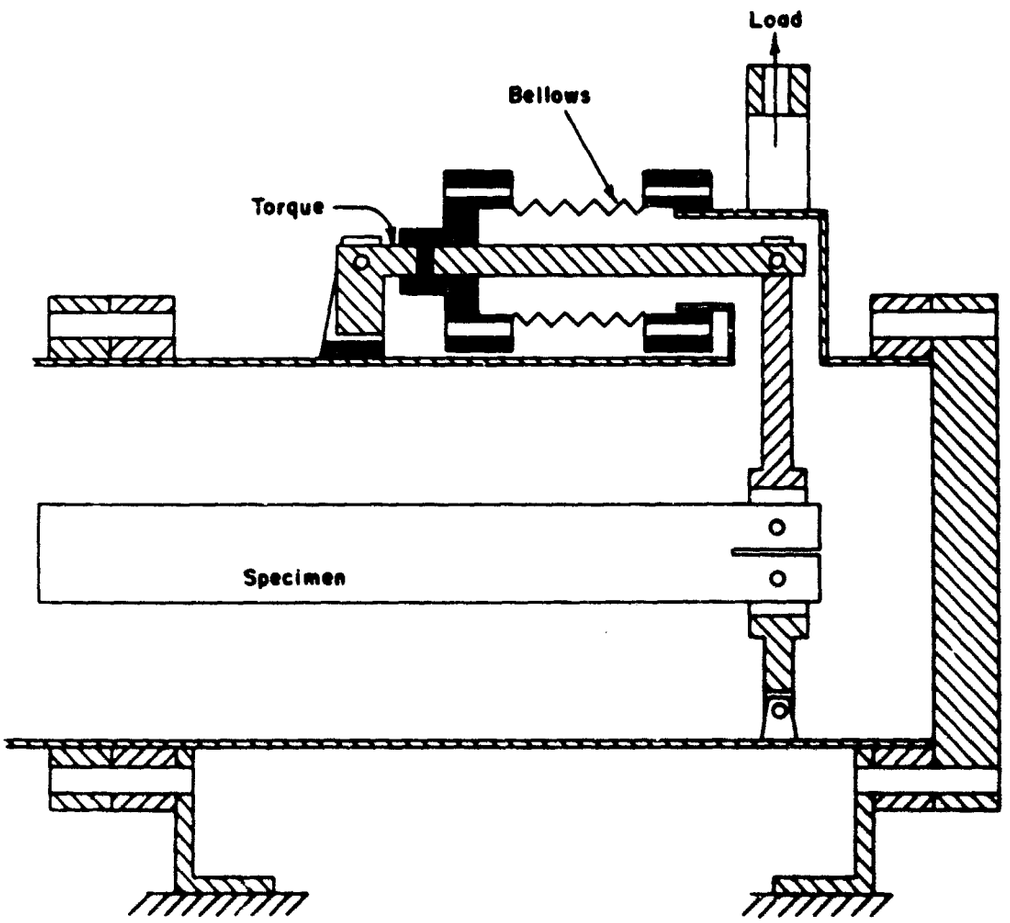

Figure 15. High Vacuum Chamber

FEED-THROUGH ASSEMBLY

1. LEVER
2. LEVER YOKE
3. FLANGE BLANK
4. PIVOT YOKE
5. LIFTING YOKE

NOTE: FLANGE IS TO BE WELDED TO LEVER

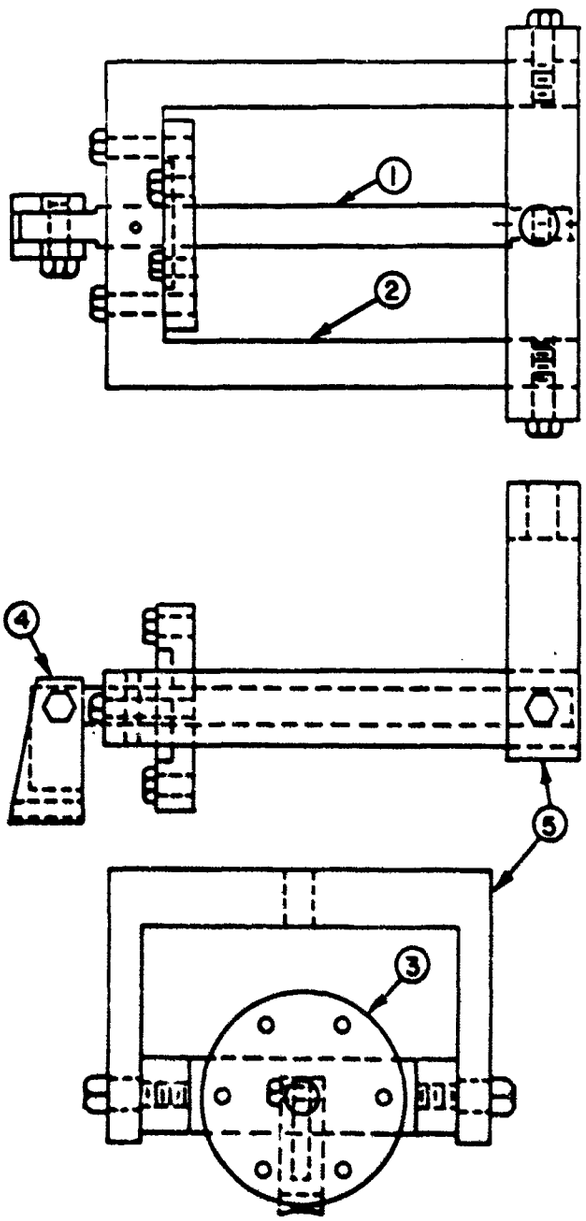

Figure 16. Feed Through Assembly

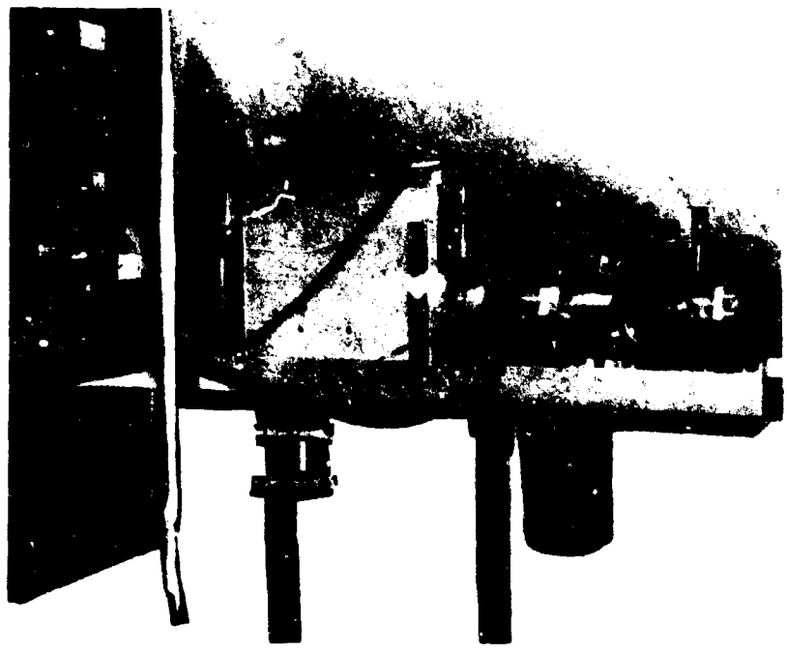

Figure 17. Assembled System.

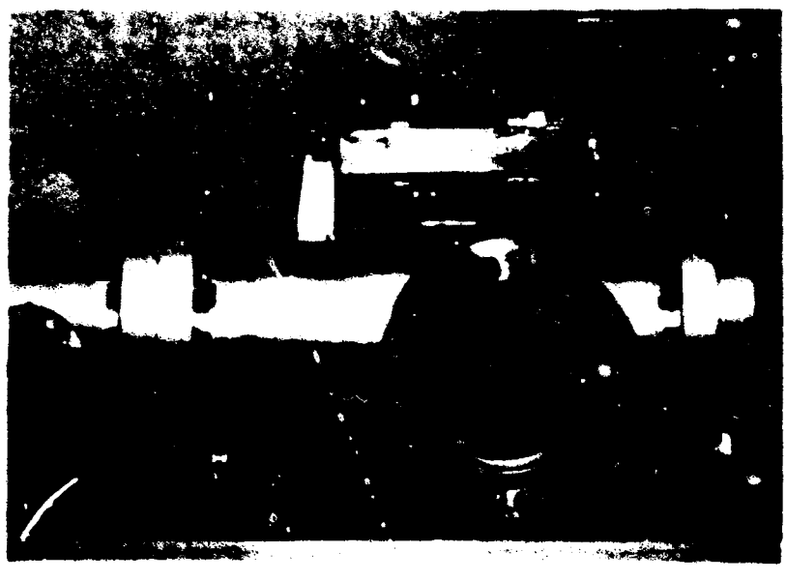

Figure 18. Specimen Chamber.

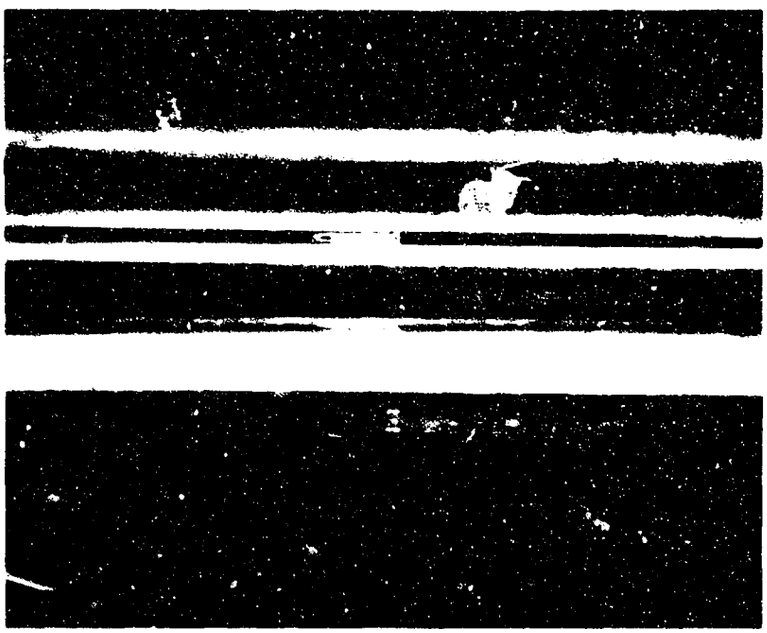

Figure 19. Cleavage Crack in Specimen.

However even without the sublimator the system regularily reached the 10^{-11} Torr range in less than 24 hrs. With the sublimator, values of 10^{-12} should be attainable.

We have tested 7 or 8 glass cleavage specimens. These were of the same material and geometry as those previously cleaved in air by Matthews and Plunkett (R. B. Matthews, M.S. Thesis, University of Denver 1967).

In a typical specimen a cleavage crack could be propagated steadily and quite smoothly (on a macroscopic scale) at loads of less than 20 lbs and various strain rates. The progress of the crack was easily observed through the viewing port. Our initial tests were to apply cyclic loads at a constant strain rate. We also loaded an identical specimen but without a cleavage crack --- in an identical manner to determine mechanical hysteresis in the linkage and to get an idea of the stiffness of the loading element. In order to make the results quantitative the system needs to be calibrated to compensate exactly for the weight of the hardware above the specimen and for extraneous hysteresis losses.

The extent of rehealing will then be the energy to refracture a given length of crack, i.e. the area between paths (3) and (1), compared with the energy to initially fracture the same length, i.e. area between paths (2) and (1). The method could then be applied to other silicates both crystalline and noncrystalline. In particular cleavable crystalline minerals would be expected to give almost complete rehealing, as suggested by the classical work of Orowan on mica cleavage over 20 years ago.

To conclude, it is unfortunate that the second approach was not tried earlier in the program, since it appears that meaningful data can be obtained from this method. It is planned to obtain additional data with glass and with cleavable ionic materials, to contrast their behavior.

6. SAMPLE PREPARATION

The purpose of the sample preparation project was to select and procure samples of various rocks and minerals that might be indigenous to the lunar surface and, more importantly, to prepare well characterized specimens of these materials for use in other phases of the research. The various types of specimen and the uses to which they were put are described in the following paragraphs.

6.1 Powders for AFCRL Adhesion Experiments

Early in the program a fairly large quantity of olivine basalt powder was prepared for use in high vacuum adhesion studies at AFCRL. The preparation involved pulverizing the material under an inert gas environment. The experiments at AFCRL were designed to study the effect of adsorbed gases and electrostatic charge on the adhesion of the fine particles under the high-vacuum conditions of the lunar surface.

6.2 Specimens for Matching Signatures in the Infrared

Over the period September 1965 to November 1967 a total of 62 different rock and mineral samples were processed and sent to the AFCRL laboratories for measurement of their infrared spectra. Each sample was represented by the following specimens:

1. Less than 5μ powder
2. A 0-74μ sizing of particles
3. A 74-250μ sizing of particles
4. A 250-1200μ sizing of particles
5. One 40 x 15 x 4 mm plaque (rough surface)
6. One 40 x 15 x 4 mm plaque (polished surface)
7. One glass slide thin section

The reduction of the samples to the various size fractions was accomplished by jaw crushers, disc pulverizers, and ball milling except that the finest fraction was achieved by passing a portion of the 0-74 fraction through a fluid energy mill operating at a dry nitrogen pressure of 100 psig.

6.3 Specimens for Matching Signatures in the Visible

The small amounts of iron contamination introduced during processing of the four particle size fractions did not affect the infrared spectra significantly; however, this same amount of contamination was found to have a highly significant influence on measurements made in the visible. Therefore, since reliable spectral data in the visible were essential to spectral matching, an intensive study was undertaken to (a) determine the sources of the iron contamination and (b) to devise new methods of processing that would produce contaminant-free specimens.

As expected, the iron contamination was found to stem from the initial reduction of the rock and mineral fragments in both the jaw crusher and disc pulverizer. The iron picked up in these two operations was difficult to remove completely by magnetic separation and some of it persisted in the finer fractions. In the case of a quartz sample, for example, the iron pick-up was sufficient to cause a visual discoloration of the <5μ fraction. The only reduction method that was found to give satisfactory iron-free specimens was to first cut 1/8-in. thick slabs from the massive rock or mineral sample and then reduce these slabs to particles by hand grinding in a mortar and pestle made from sintered alumina. The hand grinding provided the three coarser size fractions (0-74μ, 74-250μ, and 250-1200μ). The finest fraction (<5μ) was then prepared by passing some of the hand-ground material through the fluid energy mill, the exposed metal parts of which were lined with a polyurethane coating. The iron content of a <5μ quartz sample prepared in this way was less than 2 ppm. Alumina picked up by the hand grinding in the mortar and pestle, however, was as high as 400 ppm and copper pickup from the screening operations was approximately 20 ppm. Neither of these contaminants were believed sufficiently high to interfere with the spectral measurements.

A total of 107 samples were processed by the hand-grinding technique, each sample being represented by the four particle size

fractions and one polished plaque. The samples consisted of specially selected rocks and minerals most of which were igneous in origin. All 107 samples were processed during the final year of the contract. All specimens were sent to AFCRL where the spectral measurements were made.

In addition to the processing of the samples, chemical analyses were obtained on 24 of the specimens. In most cases, however, only one to four elements were determined; i.e., complete analyses were not obtained.

6.4 Olivine Basalt Powders for DRI Sintering Studies

Fairly large amounts of olivine basalt were prepared in fine particle sizing for the DRI sintering studies. Most of this material was used to study the possibility of utilizing basalt for *in situ* technological applications on the lunar surface. The other use of the basalt powder was for the experimental sintering study.

6.5 Spectral Matching Crystals

A total of 24 polished plaques, 1 x 1 x 1/4", were furnished to AFCRL for use as spectral matching crystals. These plaques or crystals were used in a spectrometer as selective filters as an aid in identifying unknown spectral radiance sources. With the measuring system that was used, an enhanced signal resulted when the composition of the source and crystal were identical.

7. STUDY OF PROTON IRRADIATION DAMAGE BY X-RAY TOPOGRAPHY

7.1 Introduction

The purpose of this investigation was to determine the effect of proton irradiation on the structure of single crystals of α-quartz, mica and spinel, possible minerals of the lunar surface, by the method of X-ray diffraction topography.

It is well known[1,2] that the passage of high-energy charged particles through solids can cause structural damage. This damage can be in the form of primary ionization or defects such as vacancies and interstitials, thermal or displacement spikes, crowdions, and primary ionization. Proton bombardment results in primary ionization and in the creation of high-energy knock-ons. There are atoms or ions that have been knocked out of their equilibrium lattice sites and are passing through the solid with energies sufficient to displace other atoms or ions from their lattice positions by collisions. Under these circumstances, a cascade process occurs until the energy is insufficient to cause further displacements. The energy stored as point defects at the end of the cascade process is a small portion of the total available energy of the primary knock-on. The remaining energy is dissipated by lattice vibrations.

The physical effects of such lattice vibrations have been interpreted by Seitz and Koehler[3] as being manifested in raising small local volumes around the knock-on paths to high temperatures for short durations. This phenomenon is called a "thermal spike". However, Brinkman[4] proposed the transient formation of a hole (or multiple vacancy) surrounded by a region of Frenkel defects (vacancy-interstitial pairs), and farther out, a shell of interstitial atoms. In the latter stages of this "displacement spike" the holes collapse and recrystallize in the orientation of the original matrix. Regardless of which simplified model or models more nearly describe the actual case, it has been shown[5-8] that dislocation loops can be caused by clustering of vacancies or interstitials which can subsequently lower their energy by collapsing into a dislocation loop.

Loops so generated would be expected to interact with existing dislocations.

Dislocations and other lattice defects have associated strain fields that can extend out many microns.[5] It is this strain field of a defect that produces the contrast image observable by the method of X-ray diffraction topography. Lattice-parameter differences of the order of 1 part in 10^7 can be detected by this method.[9]

7.2 Experimental

X-ray topography was accomplished with a Model Y-33B X-ray microfocus generator (manufactured by Engis Equipment Company, Morton Grove, Illinois, under license from Helger and Watts, Ltd., England). A high-power cathode, producing a foreshortened spot focus 100μ square at a horizontal takeoff angle of 3°, was used in conjunction with a Lang X-ray camera (Model 8-050, Jarrell-Ash Company, Waltham, Mass.). The design of the camera and the Lang method are fully described elsewhere.[10-11] The camera consists basically of a goniometer for specimen orientation, rotation controls of θ (Bragg angle) and 2θ (counter) positioning, slit assemblies for collimation of both the primary and diffracted beams, and a precision translation stage to move the crystal and film cassette simultaneously (at the rate of 1 inch per hour) while maintaining a fixed geometry with respect to the X-ray beam. By this method the entire crystal volume is scanned by the direct beam. The projected image from the diffracted beam is recorded at near unity magnification on the film (placed perpendicular to the diffracted beam) and therefore, must subsequently be enlarged photographically. Thus, the method should be applied to crystals with low dislocation densities ($<10^6/cm^2$ and preferably much lower). Fine-grain negative films, with the attendant low speed for X-ray exposures, must be used in order to approach the geometric resolution of 1 micron. Ilford nuclear research plates, 1"x1½", emulsion type L-4 (25- and 50-μ), were used for this study. Exposed plates were developed at 0 °C to suppress emulsion grain growth.

Proton bombardment was accomplished with two sources, located at the University of Colorado (Boulder), of essentially the same design with the exception of the vacuum system and beam energy capability. The basic unit, a Colutron velocity-filter isotope separator[12,13] was constructed for the purpose of preparing targets for use in a cyclotron and for radioactive isotope separation. The ion source is of the end-extraction confined-plasma type and is at the accelerating potential. Water of high purity is used as the source of protons. Extracted ions are accelerated and focused to a spot at the collector by a conventional "three-lens" system. A velocity or Wien filter, rather than a sector magnet, is used as the analyzer, the main features of which are its small size, adjustable dispersion, and intrinsic spot focus. Two pairs of electrostatic deflection plates bend the separated beams up and then down, over a baffle situated in the center of the drift tube to eliminate contamination by neutralized ions formed in or before entering the velocity filter.

The single-crystal quartz specimens were AT cuts from oscillator-quality natural Brazilian crystals furnished by TRW Crystals, Inc., (Loveland, Colorado). The AT cut wafer surface is perpendicular to the major rhombohedron[14] the Miller-Bravais indices of which are $(10\bar{1}1)$. The proton beam was normal to the specimen surface and hence parallel to the $(10\bar{1}1)$ lattice planes. The spinel ($Mg\ Al_2\ O_4$) specimens were natural octahedrons (from Ceylon), saw-cut parallel to the (111) octahedral surface, and subsequently polished with 0.05μ AB gamma alumina and a silk polishing cloth. The muscovite mica, $K\ Al_2\ (Al\ Si_3\ O_{10})\ (OH)_2$, specimens were basal cleaned (001) from an X-ray analyzer crystal.

The experimental procedure was to obtain transmission topographs of the prepared specimens prior to proton bombardment to determine their imperfection content, and thus aid in the selection of the appropriate crystals and areas for subsequent proton irradiation and in the interpretation of proton damage. Following the preliminary topography, specimens were masked with slotted Sn sheet

material to permit selected-area bombardment. The Sn mask functioned also as the charge collector during irradiation. After proton bombardment, transmission topographs were again obtained using the same Bragg reflecting planes.

7.3 Discussion and Results

The images of imperfections in crystals by X-ray diffraction topography are usually more complicated than those observed by transmission electron microscopy; however, the interpretation of the observed diffraction contrast is often similar for both cases when kinematical and dynamical theory is applied. Authier[15] has reviewed the origins and types of contrast observed with the different topographic methods. Summaries of the dynamical theory have been written by James,[16] Zachariasen,[17] and Kato,[18] and more recently by Batterman and Cole.[19] The resolution attainable in X-ray topographs is limited to about 1 micron under ideal conditions, and hence cannot compete with electron microscopy in this respect. However, certain compensating simplifications exist, some very valuable, which are intrinsic to X-ray methods.[20] Notable among these are that the volume properties of a crystal can be studied non-destructively and that a single desired Bragg reflection, and that one only, is active in producing the topograph image.

The specimens of Figures 20, 22 and 23 were irradiated in the 30-keV accelerator having an oil-diffusion pumping system capable of achieving a vacuum of 5×10^{-6} Torr during irradiation. The quartz specimen of Figure 21 was irradiated in the 125 keV accelerator having a vac-ion-sorption system capable of an operating vacuum of 2×10^{-7} Torr. The specimens of Figures 20, 22 and 23 exhibited a general surface discoloration (yellow to brown) in the irradiated area, when examined visually. All visual traces could subsequently be removed by careful swabbing of the specimen surface with acetone. The discoloration is attributed to diffusion-pump oil (or its cracked species) that has been transported with

(a)

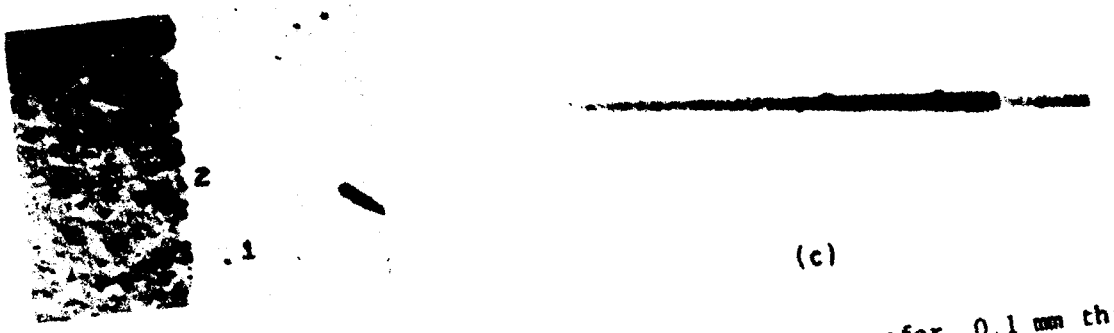

(b)

(c)

Figure 20. X-ray transmission topographs of a quartz wafer, 0.1 mm thick, (10$\bar{1}$1) reflection, after irradiation of the control portion with 30 keV protons to a dosage of 4.2×10^{16} protons/cm^2; (a) scanning topograph of crystal volume, (b) enlargement of area C of (a) showing irradiation boundary, (c) section topograph at position S-S of (a).

Figure 21. X-ray transmission topograph of a quartz wafer, 0.1 mm thick, (10$\bar{1}$1) reflection, after selective irradiation with 50 keV protons to a dosage of 1.5×10^{16} protons/cm^2.

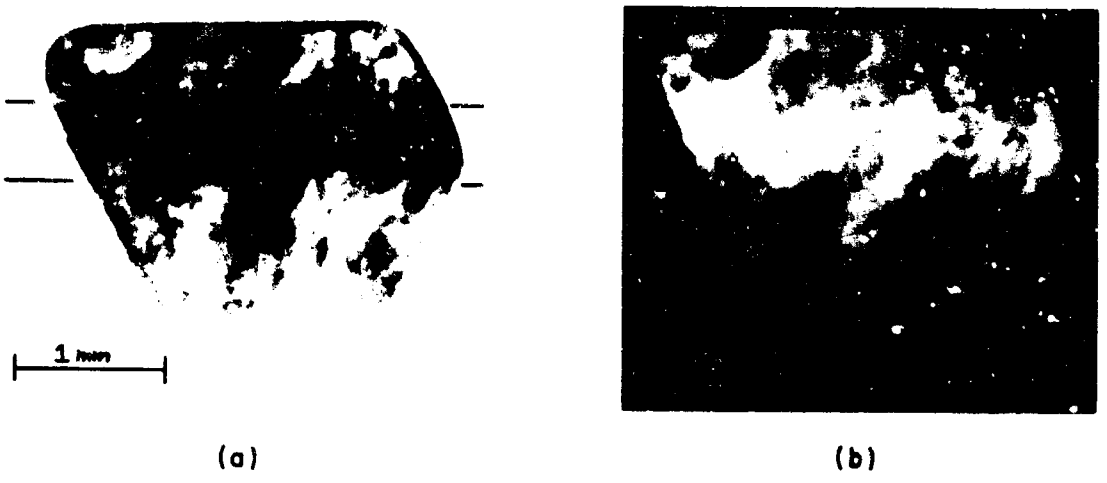

Figure 22. X-ray transmission topograph of an octahedral slice of spinel, 0.3mm thick, (311) reflection, after irradiation, within the horizontal band indicated, with 30 keV protons to a dosage of 3.6×10^{16} protons/cm^2. (b) is a positive print of (a).

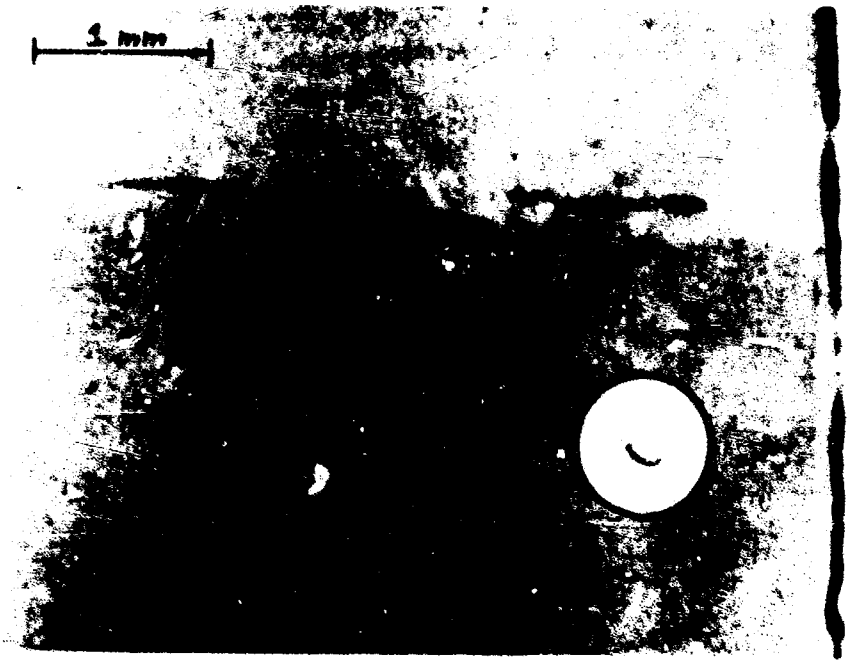

Figure 23. X-ray transmission topograph of a cleavage slice of muscovite mica, (0006) reflection, after irradiation with 30 keV protons to a dosage of 4.2×10^{16} protons/cm^2. Note the dislocation loop shown in the inset at B.

the proton beam. No such discoloration was evident after proton irradiation of the quartz specimen of Figure 21.

The proton irradiated areas of all specimens have exhibited a generalized increase in diffraction contrast. It is unlikely that the observed increased contrast is attributable at least to any significant extent, to surface contamination by diffusion-pump oil or sputtered Sn from the mask (an electron microprobe scan scross the irradiated region of the quartz crystal of Figure 21 failed to show a detectable amount of tin). Rather the observed contrast is likely attributable to lattice dilatation (highly anisotropic in the case of α-quartz) resulting from the addition of vacancies and interstitials. (Ref. 14, p.141).

Figure 20a shows the proton bombarded central region or band quite distinctly. The topograph was obtained using the $(10\bar{1}1)$ reflection, Ag $K\alpha_1$ X-radiation, a tube voltage of 45 KV, a tube current of 7.4ma, and a 24-hour exposure. The most notable features of Figure 20 are the dark doublets at A and A', the loop configurations at B and B', and the linear series of doublets at the proton irradiated boundary of area C shown enlarged at (b). It is apparent that the density of such doublets is several times greater in the bombardment region of the crystal than in the non-irradiated regions to the left and right of the circular quartz wafer. The doublets are believed to be dislocation loops portions of which are inclined to the Bragg reflecting plane $(10\bar{1}1)$ and hence non-reflecting. Uniform contrast would be observable around the entire dislocation loop if it were lying parallel to the $(10\bar{1}1)$ plane. Hirch[21] et al., have observed similar double lines in quenched aluminum, by electron microscopy, which they interpret as dislocation loops. Makin[22] has observed similar effects, which he interprets as interstitial loops, in copper irradiated with 2.5×10^{18} f.n. cm^{-2}. Figure 20 (c) is a section topograph (crystal and film not translated) at the position S-S of part (a), and illustrates that the doublets are distributed within the crystal volume.

The quartz specimen of Figure 21 was irradiated with more energetic protons (50 keV versus 30 keV of the specimen of Figure 20) but to only a third of the total dosage. Doublets similar to those of Figure 20 are also observed in the irradiated diagonal band, shown at A and B of the inset of Figure 21. Note that the proton irradiation boundaries are of higher contrast than the boundaries shown in the previous topograph. The line at C of Figure 21 is a surface scratch and the dark spots at D are fiducial marks.

The spinel topograph of Figure 3 shows a high dislocation density and hence individual defects are not resolvable; however, the region of enhanced contrast, corresponding to the horizontal band of proton irradiation is observable in (a) and perhaps is more apparent in the positive print in (b). A more nearly perfect spinel single crystal and/or one of less thickness would be more suitable for determining the extent of proton damage.

The cleavage slice of mica, 0.1mm thick, shown in the topograph of Figure 23, contains a single discernable dislocation loop at B and a linear contrast boundary at A in addition to the increased contrast in the area of irradiation below A. None of these features existed prior to proton bombardment. What appears to be a dislocation network is barely visible in the irradiated region.

This study has demonstrated that proton irradiation can indeed cause structural damage in single crystals of quartz, mica and spinel. A desirable extension of the present work would be to learn more of the nature of the effects observed; such as, the determination of the Burgers vector of the dislocation loops (by observing contrast changes with different Bragg reflecting planes), and irradiation at higher dosages to quantitatively determine the growth or shrinkage of such loops.

8. PERSONNEL

This program has been in effect for a number of years and a large number of people have been involved in various phases of the work. The personnel involved in the various programs which have been described in this report are as follows.

2. Lunar Infrared Emission Studies: D. G. Murcray, F. H. Murcray, and W. J. Williams.

3. Ion Bombardment Apparatus for Lunar Surface Simulation Studies: R. C. Amme and T. G. Clapp.

4. Sintering Studies: W. C. Hagel and J. D. Plunkett.

5. Surface Properties: P. Predecki, J. D. Plunkett, and R. B. Matthews.

6. Sample Preparation: D. G. Moore and J. D. Plunkett.

7. Study of Proton Irradiation Damage by X-Ray Topography: W. C. Hagel and R. F. Geisendorfer.

REFERENCES

Section 2.

1. Murcray, Murcray, and Williams, AFCRL-67-0448, Scientific Report No. 1, Contract AF 19(628)-4797 (July 1967).
2. Van Tassel, Icarus 8, 486 (1968).
3. Hunt and Salisbury, "Mid-infrared Spectroscopic Observation of the Moon," Philosophical Transactions Royal Soc. (in press), (1968).
4. Conel, "Infrared Emissivities of Silicates: Experimental Results and a Cloudy Atmosphere Model of Spectral Emission from Condensed Particular Mediums," J.G.R. (1969) (accepted for publication)

Section 3.

1. Thoneman, Nature 158, 61 (July 1946).
2. Moak, Reese, and Good, Nucleonics 9, No. 3 (Sept. 1951).
3. Barnfield, Farmery, Hobbis, Nelson, and Thomson, J. Nucl. Energy C4, 89 (1962).
4. McCracken, Maple, and Watson, Rev. Sci. Inst. 37, No. 7, 860 (July 1966).
5. Archard, British J. Appl. Phys. 7, 330 (Sept. 1956).
6. Vine. British J. Appl. Phys. 1., 408 (Sept. 1960).
7. Camac, Rev. Sci. Inst. 22, 197 (March 1951).
8. Cross, Rev. Sci. Inst. 22, 717 (Oct. 1951).
9. Bullock, Am. J. Phys. 23, 264 (1955).
10. Enge, Rev. Sci. Inst. 30, 248 (April 1959).

Section 5.

1. Ryan and Baker, ASTM STP, 431 (1967).
2. Timoshenko and Goodier, Theory of Elasticity (1951).

References - Section 5 Cont'd.

3. Sternberg and Rosenthal, J. Appl. Mech., 19, 413 (1952).

4. Pelloux, Boeing Scientific Research Lab. Personal Communication.

5. Gross, Technical Documentary Report No. ASD-TDR-63-605, Pt. 1 (1963).

Section 7.

1. G. J. Dienes and G. H. Vineyard, Radiation Effects in Solids, Interscience, New York, (1957).

2. G. H. Vineyard, Radiation Effects in Inorganic Solids, Discussions Faraday Society, No. 31, (1961).

3. F. Seitz and J. S. Koehler, Solid State Physics, 2, Academic Press, N. Y., (1956).

4. J. A. Brinkman, American J. Physics 24, 246ff, (1956).

5. C. S. Barrett and T. B. Massalski, Structure of Metals, 3rd Ed., McGraw-Hill (1966).

6. J. Weertman and J. R. Weertman, Elementary Dislocation Theory, Macmillan, New York, (1964).

7. H. G. Van Bueren, Imperfections in Crystals, Amsterdam: North-Holland Publishing Co., (1960).

8. R. S. Barnes, Clusters of Point Defects in Irradiated Metals, in Radiation Effects in Inorganic Solids, Discussions Faraday Society, No. 31, p.38 (1961).

9. A. R. Lang, Crystal Growth and Crystal Perfection: X-ray Topographic Studies, Discussions Faraday Society, No. 38, p. 292 (1964).

10. A. R. Lang, Crystal Imperfections by X-Ray Diffraction, Report AD 638530, Available CFSTI, 134pp. (1966).

11. A. R. Lang, J Appl. Phys. 30, p.1748 (1959).

References - Section 7 Cont'd.

12. L. Wahlin, The Colutron, A Zero Deflection Isotope Separator, Nucl. Inst. and Meth., 27 (1) (1964).

13. L. Wahlin, The Colutron Mark II, A Velocity Filter Isotope Separator, Nucl. Inst. and Meth., 38, p.133-139 (1965).

14. C. Frondel, Dana's The System of Mineralogy, Vol. III, Silica Minerals, 7th Ed., John Wiley and Sons, New York (1962).

15. A. Authier, Contrast of Dislocation Images in X-Ray Transmission Topography, in Advances in X-Ray Analysis, Vol. 10, Newkirk and Mallett (editors), Plenum Press, New York (1967).

16. R. W. James, The Optical Principles of the Diffraction of X-Rays, G. Bell and Sons, London, (1950).

17. W. H. Zachariasen, Theory of X-Ray Diffraction in Crystals, John Wiley and Sons, Inc., New York (1945).

18. N. Kato, J. Phys. Soc. Japan 7, p.397 (1952).

19. B. W. Batterman and H. Cole, Dynamical Diffraction of X-Rays by Perfect Crystals, Rev. Mod. Phys., 36(3) (1964).

20. C. S. Barrett and T. B. Massalski, Structure of Metals, 3rd Ed., McGraw Hill (1966).

21. Hirch, Silcox, Smallman and Westmacott, Dislocation Loops in Quenched Aluminum, Phil. Mag. 3, p.897 (1958).

22. M. J. Makin, The Obstacles Respondible for the Hardening of Neutron Irradiated Copper Crystals, U. K. Atomic Energy Authority Research Group. Report AERE-R-5788, Harwell, Berkshire (1968).

Unclassified

DOCUMENT CONTROL DATA - R & D

Security classification of title, body of abstract and indexing annotation must be entered when the overall report is classified.

University of Denver Department of Physics Denver, Colorado 80210	Unclassified 2b. GROUP

3. REPORT TITLE

LUNAR SURFACE STUDIES

4. DESCRIPTIVE NOTES (*Type of report and inclusive dates*)

Scientific, Final, 17 May 1965 through 15 January 1969, Approved: 18 Mar. '69

5. AUTHOR(S) (*First name, middle initial, last name*)

David G. Murcray

6. REPORT DATE	7a. TOTAL NO. OF PAGES	7b. NO. OF REFS
January 1969	64	41

8a. CONTRACT OR GRANT NO	9a. ORIGINATOR'S REPORT NUMBER(S)
AF 19(628)-4797 b. PROJECT ~~NO~~ Task, Work Unit Nos. 8602-02-01 c. Dod Element 61445014 d. Dod Subelement 681311	9b. OTHER REPORT NO(S) (*Any other numbers that may be assigned this report*) AFCRL-69-0089

10. DISTRIBUTION STATEMENT

1-Distribution of this document is unlimited. It may be released to the Clearinghouse, Department of Commerce, for sale to the General Public.

11. SUPPLEMENTARY NOTES	12. SPONSORING MILITARY ACTIVITY
TECH, OTHER	Air Force Cambridge Research Laboratories (CRF) L. G. Hanscom Field Bedford, Massachusetts 01730

13. ABSTRACT

This report presents the results of a number of investigations, the common goal of which was a better understanding of the lunar surface. These studies have included measuring the infrared emissivity of various areas of the lunar surface in the wavelength region from 7μ to 14μ with a balloon borne system and laboratory studies of the benavior of various materials under simulated lunar environment. The laboratory studies have included the role of sintering in the mechanical properties of lunar surface, techniques for measuring the adhesive properties of fresh surfaces in a high vacuum environment, development of proton beams which can give reasonable proton fluxes in a high vacuum environment for the study of the effect of protons on lunar surface materials and finally the possibility of using X-ray topography as a tool for studying proton damaged surfaces.

DD FORM 1 NOV 65 1473 (PAGE 1)

S/N 0101-807-6801

Unclassified

Security Classification

14 KEY WORDS	LINK A		LINK B		LINK C	
	ROLE	WT	ROLE	WT	ROLE	WT
Lunar Surface						
Infrared Emission						
Lunar Spectrum						
Ion Bombardment Apparatus						
Protons						
Heavier Ions						
Ultrahigh Vacuum						
Sputtering						
Ion Optics						
Luminescence						
Silicates						
Creck Initiator						
Rehealing						
Cyclic Loading						
Sintering						
Basalt						
Viscous Flow						
Necking Curvatures						
Silicate Powders						
Size Fractions						
Chemical Analyses						
Polished Plaques						